

Department of Marine, Earth and Atmospheric Sciences, North Carolina State University, Raleigh, NC

Mesoscale simulations of dynamical factors discriminating between a tornado outbreak and non-event over the southeast US Part III: 6 hour precursors

J. M. Egentowich, M. L. Kaplan, Y.-L. Lin, and A. J. Riordan

With 27 Figures

Received December 23, 1999

Revised January 16, 2000

Summary

Using observational analysis and mesoscale numerical simulations we investigate the subtropical jet (STJ) and the associated mass and momentum adjustments, the low-level jet (LLJ), and low-level potential vorticity (PV), 6 hours before the 1988 Raleigh (RDU) tornado outbreak. We also compare the environment to a synoptically similar event with severe weather forecasted but nothing developed over central North Carolina.

In the event case there is a self-maintaining, low-level circulation, which was characterized by a surface trough, low-level PV maximum, mid-level jet and a warm Mexican airmass, that originated over Mexico, propagated across the Gulf Coast and moved over central North Carolina at the time of tornado. A meso-cyclone and low-level PV propagates over the Piedmont at the time of the RDU tornado outbreak. The low-level PV maximum is maintained by low-level forcing: specifically, tilting about a diabatic heat source (convection). In the non-event case, this feature is absent along the Gulf Coast states. In the event case, the polar jet right entrance region moves near the STJ left exit region which creates strong ascent and upper-level divergence over the Piedmont. The lifted index indicates the airmass over the Piedmont is unstable. We developed a Divergence Profile Buoyancy Index (DPBI) based on: upper-level divergence, airmass buoyancy and low-level tilting effects associated with shear and thermal gradients. We found that DPBI values over 15 correspond to tornadic activity.

1. Introduction

In this final part of this three part series of papers, we examine the last 6 hours before a severe weather event and compare it to a synoptically similar non-event. Egentowich et al. (1999a) (in this issue Part I) compared the event (RDU tornado, 28 November 88) to the non-event (25 January 1990), and discussed the early synoptic situation (84-48 hours before hand), jet development, low-level PV development and warm air transport. The event and non-event cases were synoptically very similar for the 48 hours preceding the event case. Before the 48-hour point the synoptic situations contained notable differences. Seventy-two hours before the event, a STJ streak over TX and MX helped create a low-level trough and low-level jet (LLJ) over the western Gulf of Mexico. The non-event case had a different synoptic pattern; the upper-level flow was zonal over the US with a ridge over MX, which prevented the development of a STJ or LLJ.

In the event case, low-level PV was generated in the upper levels and transported to the midlevels (~ 500 hPa) by the thermally indirect

circulation associated with the STJ exit region where it was maintained by a mountain-plains solenoid. A hydrostatic mountain wave transported the PV to the low-levels and the LLJ transported the PV northeastward along the Gulf Coast. In the non-event case, the STJ was absent, thus PV was not transported downward to the midlevels. The easterly low-level flow prevented the development of mountain waves and advected moist air over the Mexican plateau, which inhibited the development of a mountain plains solenoid.

Egentowich et al. (1999b) (in this issue Part II) compared the time period 48 to 6 hours before the event and the non-event. In the event case, a surface trough, low-level PV maximum, mid-level jet, a warm Mexican airmass and STJ exit region were co-located and moved across the Gulf Coast states as an entity. Also, the STJ exit region created upper-level divergence and ascent in the left exit region, which helped to maintain a low-level trough. The warm Mexican airmass was located over the Gulf Coast (southeast of the surface trough) and facilitated the development of a mid-level, northwestward directed pressure gradient force (PGF) and a mid-level jet. These features created an environment favorable to deep convection. The PV maximum propagated eastward across the Gulf then to the Piedmont at the time of the RDU tornado and was maintained in the low-levels by tilting effects. These features interacted to produce a self-sustaining feature that moved across the northern Gulf Coast of the US and over central NC at the time of the tornado. In the non-event case, these features were absent along the Gulf Coast.

In these papers, we compare the RDU tornado event to a synoptically similar non-event where severe weather was forecasted but none developed over central NC. The Raleigh NWS (Gonski, personal communication, 1998) expected severe weather to develop over central NC at 1800 UTC (designated as the onset of the non-event). The convective outlook and second day severe outlook were forecasting severe thunderstorms across the Piedmont, with possible isolated tornadoes over GA. In fact, at 1437 UTC, the National Severe Storms Forecast Center (Kansas City) issued a severe thunderstorm watch for central GA, SC and NC valid from 1400 to 2000 UTC. The window of the non-event ends when a front moves over

central NC near 0000 UTC 26 January 1990. Since the actual time of the non-event is ambiguous, we will examine the non-event over a period of time starting at 1800 UTC 25 and ending 0000 UT 26 January 1990.

In this paper, we explore the relationship between the existence of the STJ and its effects on the lower-layer environment over the last 6 hours before the severe weather outbreak. We also compare the environment to a synoptically similar non-event case. In Section 2 we will briefly describe the mesoscale model used for the simulations. Section 3 deals with the development of the upper-level jet streaks. Section 4 focuses on the development and movement of the mid-level jet. In Section 5 we will investigate the transport of the low-level PV. Section 6 describes the low-level environment conducive to severe weather over the Carolina Piedmont. In Section 7 we describe a new Divergence Profile Buoyancy Index (DPBI). Finally, in Section 8 we will summarize and present our conclusions.

2. Model summary

Due to the lack of high-resolution observational data, numerical simulations are employed to understand the environments prior to the event and non-event. The MASS model (Kaplan et al., 1982) version 5.8 (MESO, 1995) is employed for the simulations in this study. The numerical model specifics and experiments are summarized in Part I. For this study, we use a larger 24 km grid ($205 \times 155 \times 40$) with both the 24 km and 12 km grids shifted to the northeast, centering NC in the simulation domain. Three-dimensional parcel trajectories used in this paper are derived from the Mesoscale Atmospheric Simulation System Trajectory software package (Rozumalski, 1997).

3. Upper-level jet development

The PJ streak and STJ streak development over the 24 hour period before the event and non-event is described in Kaplan et al. (1995). At 0000 UTC 28 November 1988, the NWS analysis (Fig. 1a) depicts the exit region of the STJ over the Piedmont. There is supergeostrophic flow over the VA, NC and SC coastal region. At the same time, the PJ moves to the west of the Appalachians

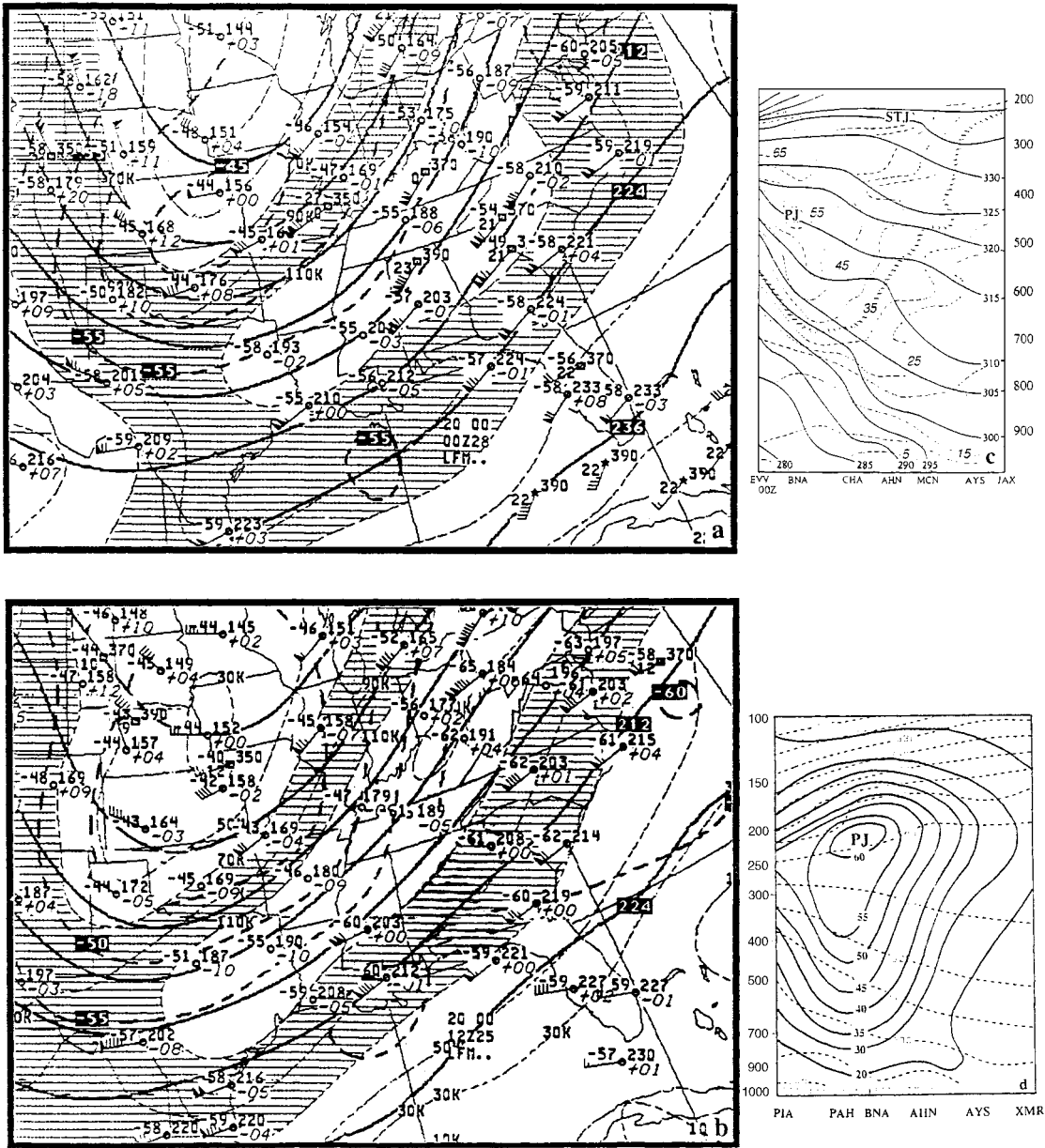


Fig. 1. **a** NWS 200 hPa analysis of isotachs (knots) and vectors, temperature (C) and height (dm), and **c** observationally derived cross section from Evansville, IN (EVV) to Jacksonville, FL (JAX), isotachs (dashed line, ms^{-1}) and θ (solid line, K) valid at 0000 UTC 28 November 1988; **b** NWS 200 hPa analysis of isotachs (knots) and vectors, temperature (C) and height (dm), and **d** observationally derived cross section from Peoria, IL (PIA) to Cape Kennedy, FL (XMR) isotachs (solid line, ms^{-1}) and θ (dashed line, K) valid at 1200 UTC 25 January 1990

thus the PJ's right entrance region comes in close proximity to the STJ's left exit region. The associated transverse ageostrophic jet streak circulations are arranged so that a region of intense ascent develops between the jet streaks and over the Piedmont. At 1200 UTC 25 January

1990, the NWS analysis (Fig. 1b) depicts that a PJ extends from TX northeast to the north Atlantic Ocean, with supergeostrophic flow over the entire East Coast. There is no STJ over the eastern US; thus no jet streak phasing occurs. Figure 1c and d depict a cross section bisecting

the jets. In the event case, two jet streaks are present, while only one is present in the non-event case.

3.1 Model simulated cross sections for event and non-event cases

Model generated cross sections are perpendicular to the jet streaks over the Piedmont extending from southern OH (39N, 83W) to the Atlantic Ocean, east of SC (33N, 75W). The first event case cross section is valid at 0100 UTC 28 November 1988 (Fig. 2a). At this time, the STJ streak has not entered the cross section, it is still located to the southwest. Also, the PJ entrance

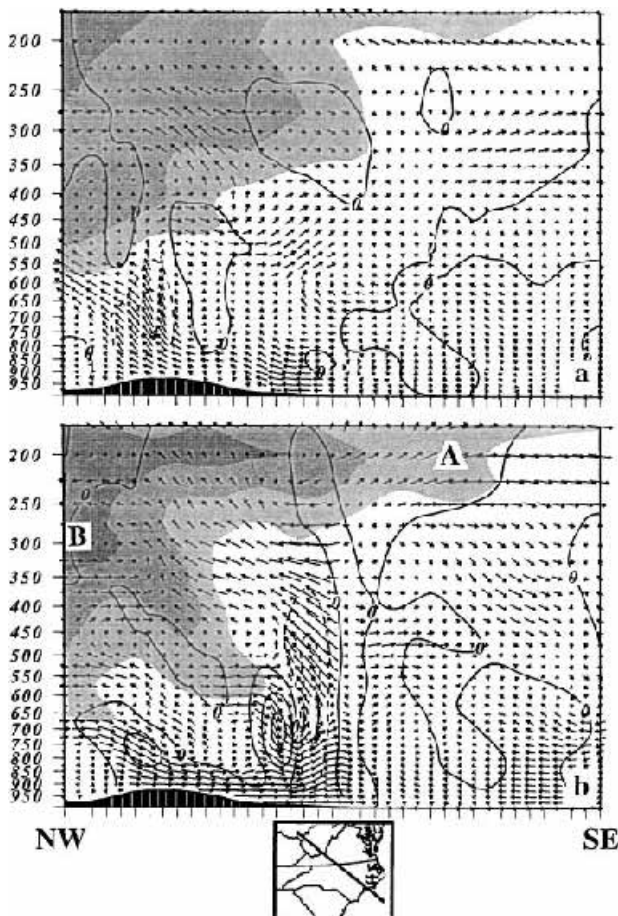


Fig. 2. MASS simulated, 24 km mesh, cross sections extending from (38N, 93W) to (33N, 75W). Includes ageostrophic wind vectors, wind isotachs (shaded at intervals of 10 for speeds greater than 40), and vertical velocity (contoured every $20 \mu\text{b s}^{-1}$, solid lines indicate descent and dashed lines indicate ascent) valid at **a** 0100 UTC, and **b** 0600 UTC 28 November 1988. A denotes the STJ and B denotes the PJ

region is nearing the cross section so the thermally direct ageostrophic circulation is not well defined. The ageostrophic circulation extends to the surface. There is strong organized ascent from the surface to the 300 hPa level with a maximum value near the 700 hPa level. The jet streaks and upward vertical velocity are over the Appalachian Mountains.

At 0600 UTC 28 November 1988 the PJ streak entrance region is located to the west of RDU and the STJ streak exit region is located to the east of RDU. The 0600 UTC cross section (Fig. 2b) depicts ageostrophic motions and ascent over the Piedmont. The subtropical jet exit region is depicted as a velocity bulge that extends over the 200 hPa level (A) with a strong southeastward-directed ageostrophic wind (near the 200 hPa level). The PJ extends from 250 to 450 hPa (B) with a strong northwestward-directed ageostrophic wind (200–250 hPa level). Also, there is a strong thermally direct circulation about the mid-level jet (~ 600 hPa). These ageostrophic circulations phase, which creates strong ascent over central NC.

The cross section of the non-event case valid at 1300 UTC 25 January 1990 is shown in Fig. 3a. The PJ streak core (maximum winds greater than 60 m s^{-1}) is located near the 250 hPa level (C). The bulge on the south side of the PJ core (D) could represent a transient signal of the STJ streak. Also, there is an ill-defined ageostrophic circulation around the jet streak. There is an ascent maximum over the Appalachian Mountains associated with a mid-level jet. The PJ entrance region and its associated thermally direct circulation is still to the southwest of the cross section.

The second non-event cross section is valid at 1800 UTC on 25 January 1990 (Fig. 3b). The PJ core (winds greater than 60 m s^{-1}) covers a larger area than that is the event case cross section and is located near the 300 hPa level. There is a discernible thermally direct ageostrophic circulation around the upper-level jet streak. Also, the STJ streak is noticeably absent. The ascent maximum over the Appalachians is weakening. The mid-level jet is intensifying and being assimilated into the main body of the PJ. However, the ageostrophic circulation about the jet is very weak and so is the ascent over the Piedmont.

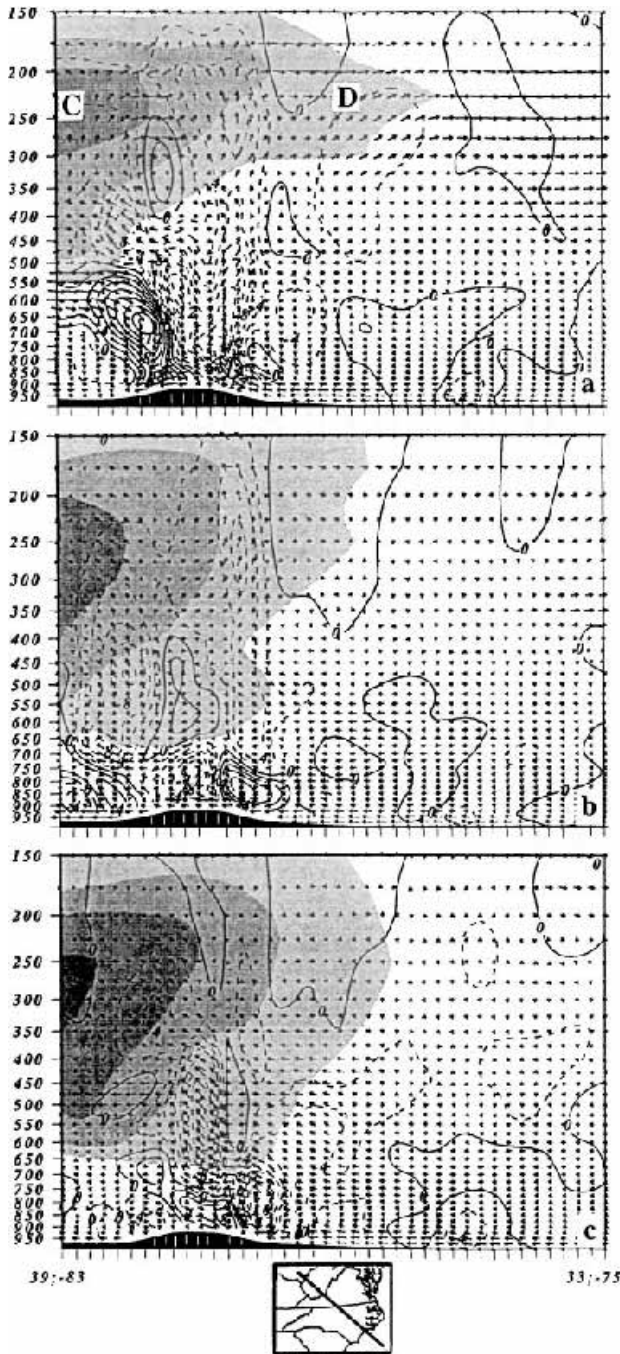


Fig. 3. MASS simulated, 24 km mesh, cross sections extending from (38N, 93W) to (33N, 75W). Including ageostrophic wind vectors, wind isotachs (shaded at intervals of 10 for speeds greater than 40 ms^{-1}), and vertical velocity (contoured every $20 \mu\text{bs}^{-1}$, solid lines indicate descent & dashed lines indicate ascent) valid at **a** 1300 UTC 25, **b** 1800 UTC 25, and **c** 0000 UTC 26 January 1990. D denotes the STJ and C denotes the PJ

The third non-event cross section is valid at 0000 UTC 26 January 1990 (Fig. 3c). The PJ core increases in strength with the maximum winds

greater than 70 ms^{-1} and covers a larger area than the previous cross section. A thermally direct ageostrophic circulation is associated with the upper-level jet streak. Six hours after the expected time of severe weather, there is weak ascending motion over the Carolina Piedmont.

3.2 Upper-level divergence

The model simulated ageostrophic circulations associated with the PJ entrance region and the STJ exit region transport mass away from the area between these two jets, which facilitates ascent and deep convection. We examine the mass removal from the upper-levels by integrating the divergence over the 375–200 hPa layer. At 0300 UTC 28 November 1988 (Fig. 4a), over eastern TN and western NC and SC, there is a large area of weak upper-level divergence as the right entrance region of the PJ approaches the left exit region of the STJ. By 0600 UTC (Fig. 4b) the two jets have superimposed in such a way as to create strong upper-level divergence and ascent over central Carolina (also depicted in the previous section). The strong upper-level divergence intensifies the ascent, which facilitates severe weather. Also, upper-level divergence is calculated at 0600 UTC (Fig. 4c) using data from a simulation with convection deactivated. As in the simulation with convection, there are upper-level divergence maxima over the Appalachians and over the central Piedmont. Convection enhances upper-level divergence; however, the juxtaposition of the PJ and the STJ predisposes the environment to strong divergence over western and central NC. In the non-event case, only the PJ exists over the southeast US. Figure 5a–c depict the upper-level divergence at 1800 UTC 25, 2100 UTC 25 and 0000 UTC 26 January 1990, respectively. The non-event case has upper-level divergence associated with the thermally direct circulation about the PJ entrance region. The upper-level divergence remains west of the Piedmont as the PJ propagates over the Appalachians.

In summary, the cross sections, upper-level divergence and backward trajectories (not shown) support the concept that the PJ, STJ and mid-level jet merge over the Piedmont in the event case. The juxtaposition of the thermally direct ageostrophic circulations (about the PJ and the mid-level jet) and the thermally indirect

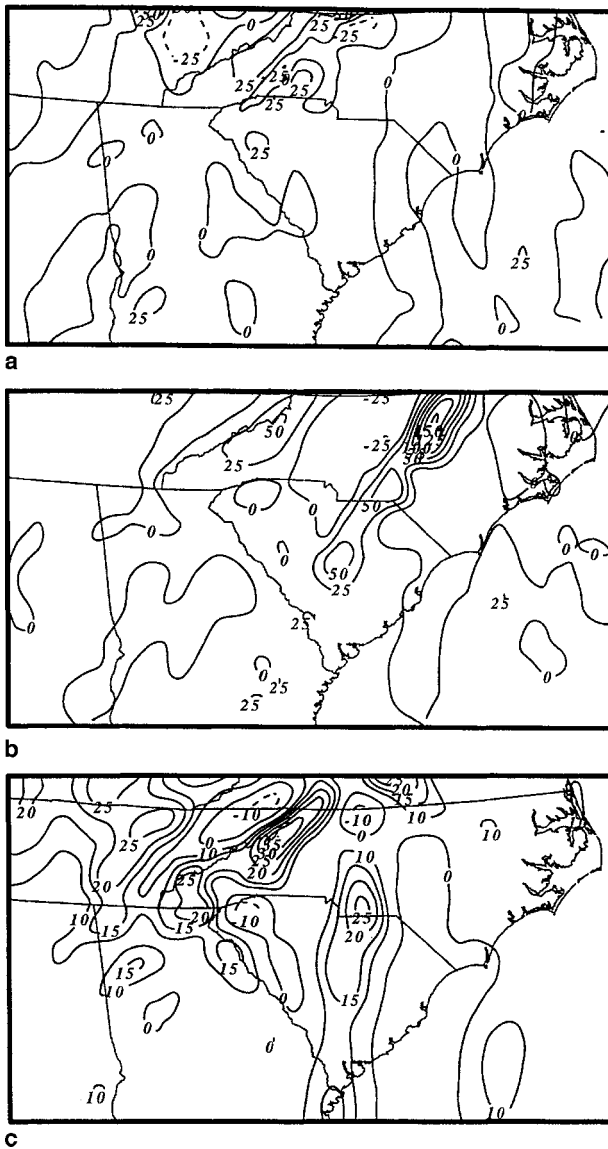


Fig. 4. MASS simulated, 12 km mesh, integrated divergence over the 375 to 200 hPa layer (solid lines indicate divergence and dashed lines indicate convergence, $\times 10^{-5} \text{ s}^{-1}$) valid at **a** 0300 UTC, **b** 0600 UTC, and **c** MASS simulated divergence field at 0600 UTC 28 November 1988 with convection deactivated

ageostrophic circulation (about the STJ) creates an area of strong upper-level divergence and ascent, which facilitates the development of deep convection and surface pressure falls.

4. Mid-level jet development

4.1 Mid-level jet development

In the event case, the simulated mid-level jet (centered near the 600 hPa level, speed

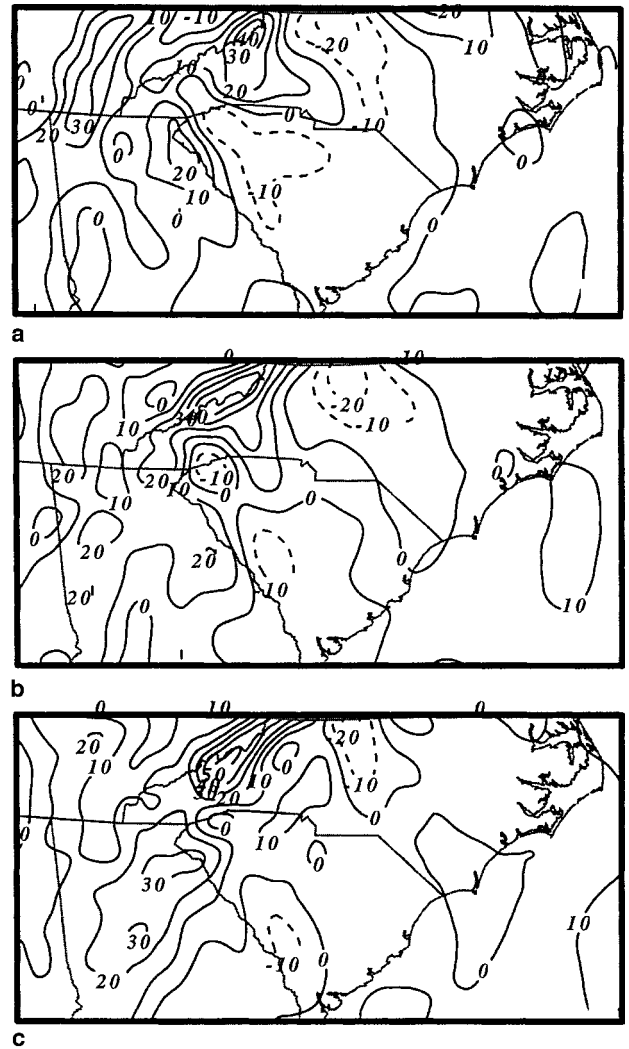


Fig. 5. MASS simulated, 12 km mesh, integrated divergence over the 375 to 200 hPa layer (solid lines indicate divergence and dashed lines indicate convergence, $\times 10^{-5} \text{ s}^{-1}$) valid at **a** 1800 UTC 25, **b** 2100 UTC 25, and **c** 0000 UTC 26 January 1990

$> 35 \text{ ms}^{-1}$) develops over the Piedmont. Figure 6 depicts the 600 hPa PGF, wind field and the 850 hPa equivalent potential temperature fields of the event case. After 0000 UTC 28 November 1988, a strong jetlet with a maximum wind speed of 50 ms^{-1} develops over central Georgia and western North Carolina. By 0600 UTC 28 November 1988, the jet streak covers most of the region. In addition, the jetlet development corresponds well with the 850 hPa thermal gradient. The warm air from MX ($> 330 \text{ K}$) at 850 hPa elevates the heights to the southeast of the mid-level jet creating a mid-level PGF. The elevated heights are in the right exit region

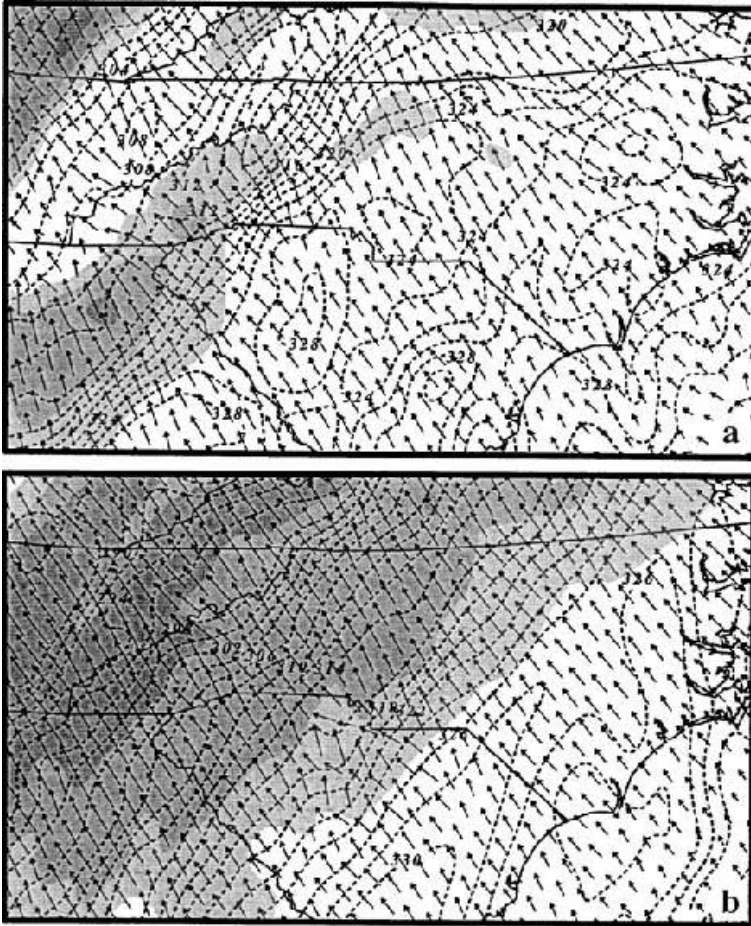


Fig. 6. MASS simulated, 12 km mesh, 600 hPa, wind isotachs (shaded at intervals of 5 for speeds greater than 35 ms^{-1}), pressure gradient force vectors (ms^{-2}) and 850 hPa θ_e (dashed lines, K) valid at **a** 0000 UTC, and **b** 0600 UTC 28 November 1988

forcing the development of an unbalanced jetlet. In the exit region, a thermally direct ageostrophic circulation develops as the atmosphere tries to balance itself. This forcing mechanism is continually regenerated as the surface frontogenesis and the low-level baroclinic zone develops, the warm MX air remains to the southeast and latent heating is generated as convection develops. The jetlet develops over the ensuing hours and moves beneath the PJ entrance region and the STJ exit region, which further enhances ascent.

For the non-event case, after 0000 UTC 25 January 1990, a mid-level jet develops with a balanced QG system west of the Piedmont (Fig. 7). The jet develops as a low pressure system intensifies over central US and this jet is closely associated with a strong height (pressure) gradient. It develops over eastern OK (extending to the northeast) and propagates northeastward. The right flank of the jet streak is over western Carolina from 1200 25 January to 0000 26

January. In contrast to the event case, the warm air from MX ($> 330 \text{ K}$) at 850 hPa has not moved over the Piedmont. The strongest thermal gradient is over the Appalachians; thus the height gradient (PGF) and mid-level jet are located to the west of the Piedmont. Also, the mid-level jet is much closer to a state of balance than in the event case. Between 1800 UTC 25 (Fig. 3b) and 0000 UTC 26 January 1990 (Fig. 3c), there is descent in the low-levels and very weak ascent in the mid-levels over the Piedmont.

4.2 Three-dimensional trajectory analysis

Three-dimensional parcel trajectories are constructed to illustrate the mid-level jetogenesis. We examine the forced adjustments imposed upon air parcels as they move through the mid-level jetogenesis region before the event and non-event cases. Figure 8 and Table 1 depicts the event case jetlet development (0000 UTC to 0400

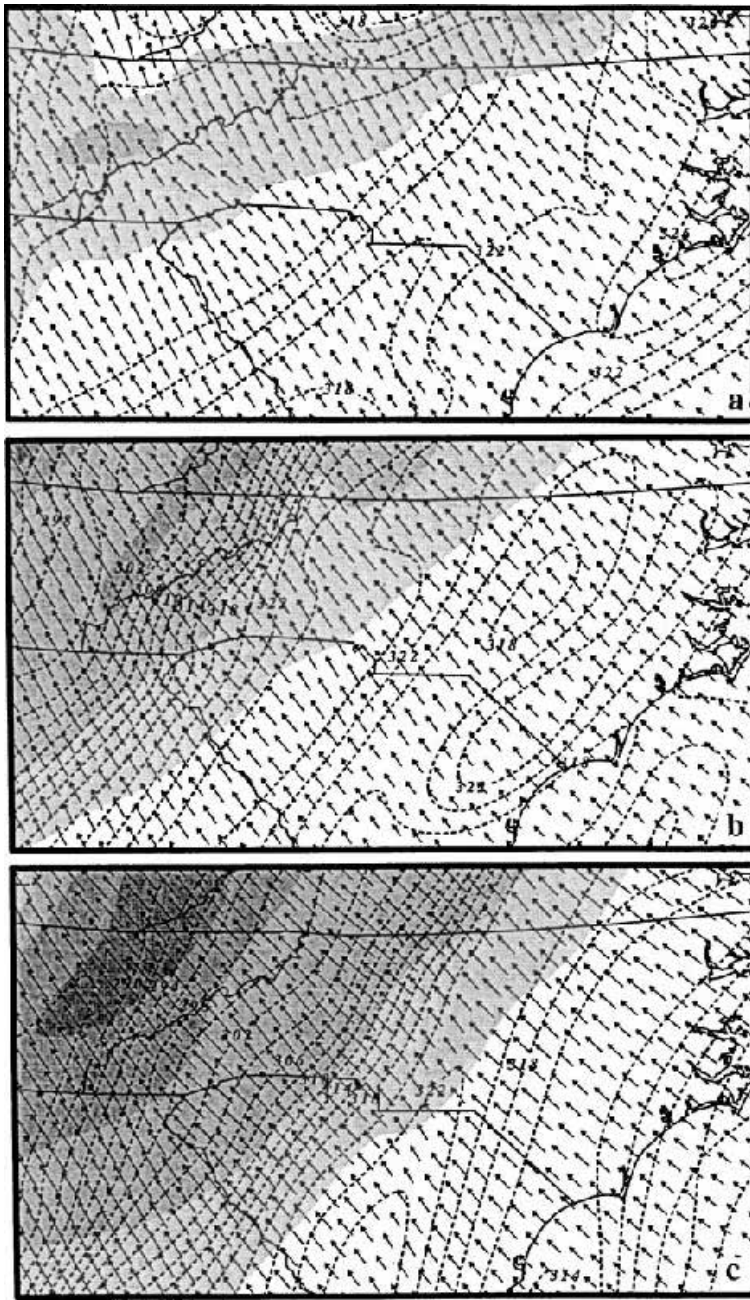


Fig. 7. MASS simulated, 12 km mesh, 600 hPa, wind isotachs (shaded at intervals of 5 for speeds greater than 35 ms^{-1}), θ_e (dashed lines, K), and pressure gradient force vectors (ms^{-2}) valid at **a** 1200 UTC, **b** 1800 UTC 25, and **c** 0000 UTC 26 January 1990

UTC 28 November 1988). The parcel originates upstream of the mid-level jet and passes through the jetogenesis area. As the parcel moves into the jetlet exit region it deflects to the left, accelerates and ascends. The higher heights to the southeast produce a northwest-directed PGF that is larger in magnitude than the opposing Coriolis force (Table 1) thus the parcels accelerate in the exit region. The leftward-directed acceleration enhances the mid-level jetlet. The Lagrangian Rossby numbers are considerably larger than 0.5

indicating unbalanced flow (Table 1). Also, the nonlinear balance equation (NBE) totals are considerably larger than 10^{-8} , which again indicates unbalanced flow because of its exit region location (Kaplan and Paine, 1977). The parcel stays on the same pressure level as it moves through the jet streak until it moves into the exit region with a thermally direct ageostrophic circulation where it begins to ascend (from 584 hPa to 490 hPa in 1 hour). The vertical velocity (Table 1) confirms that there is little

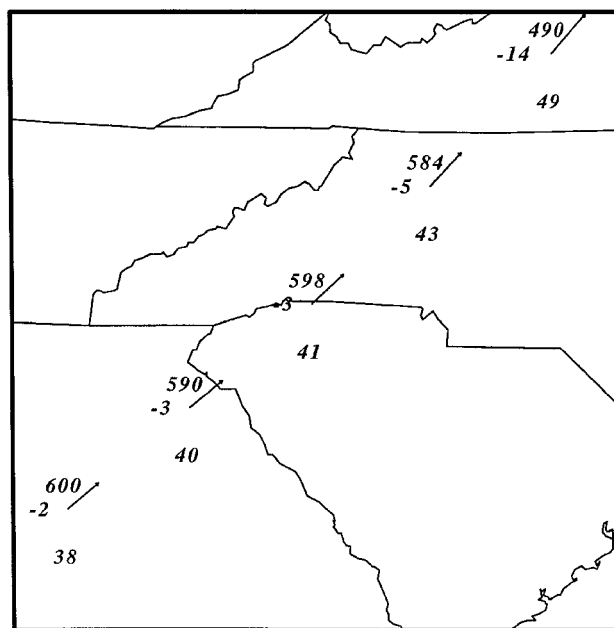


Fig. 8. Trajectory constructed from the 12 km MASS simulation initialized at 0000 UTC and ended at 0400 UTC 28 November 1988. Station plots contain pressure (hPa), temperature (C), and total wind speed (ms^{-1}). Displayed wind vectors depict total wind

ascent until the last few hours. The mid-level jet over the Carolinas is accelerating, unbalanced, and has a direct circulation of the exit region, in sharp contrast to the balanced jet dynamics (Uccellini and Johnson, 1979).

The non-event case jet development (1200 to 1600 UTC 25 January 1990) is depicted in Fig. 9a and Table 2. The parcel originates at the same

position as the event case so the parcel again passes over western NC. In the entrance region, the PGF is directed to the northwest and it is consistently larger in magnitude than the opposing Coriolis force (Table 2) thus the parcel accelerates rapidly. As the parcel moves into the jetlet exit region it decelerates and deflects to the right into an area of convergence (indicating indirect circulation). The Lagrangian Rossby numbers (Table 2) are less than 0.5, which indicates balanced flow. The NBE totals are an order of magnitude lower than the event case (near 1×10^{-8}) indicating balanced flow (Kaplan and Paine, 1977). The parcel ascends slowly as it moves through the jet streak then levels out as it moves into the jetlet exit region. The vertical velocity, parcel speed, Rossby numbers and areas of divergence surrounding the jet all indicate balanced flow. The mid-level jet over the Piedmont is decelerating, balanced, and has a thermally indirect circulation in the exit region, consistent with the Uccellini and Johnson (1979) paradigm.

The non-event case jet development from 1800 to 2200 UTC 25 January 1990 (Fig. 9b) is also examined with nearly identical results as above (data not shown). The parcel originates at 600 hPa over southern SC so the parcel passes over central North Carolina at the expected time of severe weather. As the parcel moves through the mid-level jet it accelerates from 28 to 35 ms^{-1} and ends on the 606 hPa level; the vertical velocity being essentially zero. The Lagrangian

Table 1. Forward trajectory initiated at 0000 UTC 28 November 1988 and ending at 0400 UTC 28 November 1988. Trajectory data is derived from 12 km full physics MASS model run. The following abbreviations are defined: Latitude (LAT), Longitude (LON), Pressure (PRS), Coriolis force vector (CO), Pressure gradient force vector (PGF), Lagrangian Rossby number (Ro_L), Nonlinear balance form of the divergence equation (NBE) Total wind (V_t), Omega (OMGA), and divergence computed on a theta surface (DIV)

| Time (UTC) | LAT ($^{\circ}\text{N}$) | LON ($^{\circ}\text{W}$) | PRS (hPa) | CO $\times 10^{-3} \text{ms}^{-2}$ speed/dir | PGF $\times 10^{-3} \text{ms}^{-2}$ speed/dir | NBE Total $\times 10^{-8} \text{s}^{-1}$ | V_{total} (ms^{-1}) speed/dir | Ro_L | OMGA 10^{-1}Pa s^{-1} ($\times 10^{-5}$) | Div ($\times 10^{-5}$) |
|------------|----------------------------|----------------------------|-----------|--|---|--|---|---------------|--|--------------------------|
| 28/0000 | 33.5 | 84.5 | 600 | 3.04/319 | 2.34/129 | -3.920 | 38.6/229 | *** | -1.075 | -6.548 |
| 28/0030 | 33.91 | 83.93 | 592 | 3.14/319 | 3.48/141 | 3.405 | 38.6/228 | 0.736 | -6.26 | -0.999 |
| 28/0100 | 34.33 | 83.33 | 590 | 3.27/320 | 4.2/148 | 14.73 | 39.8/230 | 0.794 | 5.128 | -2.201 |
| 28/0130 | 34.76 | 82.73 | 596 | 3.33/319 | 4.65/145 | 18.63 | 40.0/229 | 0.696 | 3.484 | 0.959 |
| 28/0200 | 35.19 | 82.13 | 598 | 3.41/317 | 9.57/127 | 12.32 | 40.6/227 | 0.714 | -2.97 | -2.418 |
| 28/0230 | 35.65 | 81.54 | 596 | 3.54/314 | 2.88/137 | -27.63 | 41.6/224 | 1.754 | -8.53 | -6.504 |
| 28/0300 | 36.13 | 80.94 | 584 | 3.71/314 | 5.3/160 | 10.416 | 43.2/224 | 1.31 | -26.04 | -0.546 |
| 28/0330 | 36.64 | 80.32 | 544 | 4.16/314 | 4.29/173 | 15.82 | 47.7/224 | 2.567 | -23.37 | 18.54 |
| 28/0400 | 37.19 | 76.69 | 490 | 4.30/313 | 4.08/143 | -2.248 | 48.8/223 | 2.002 | -26.43 | 10.73 |

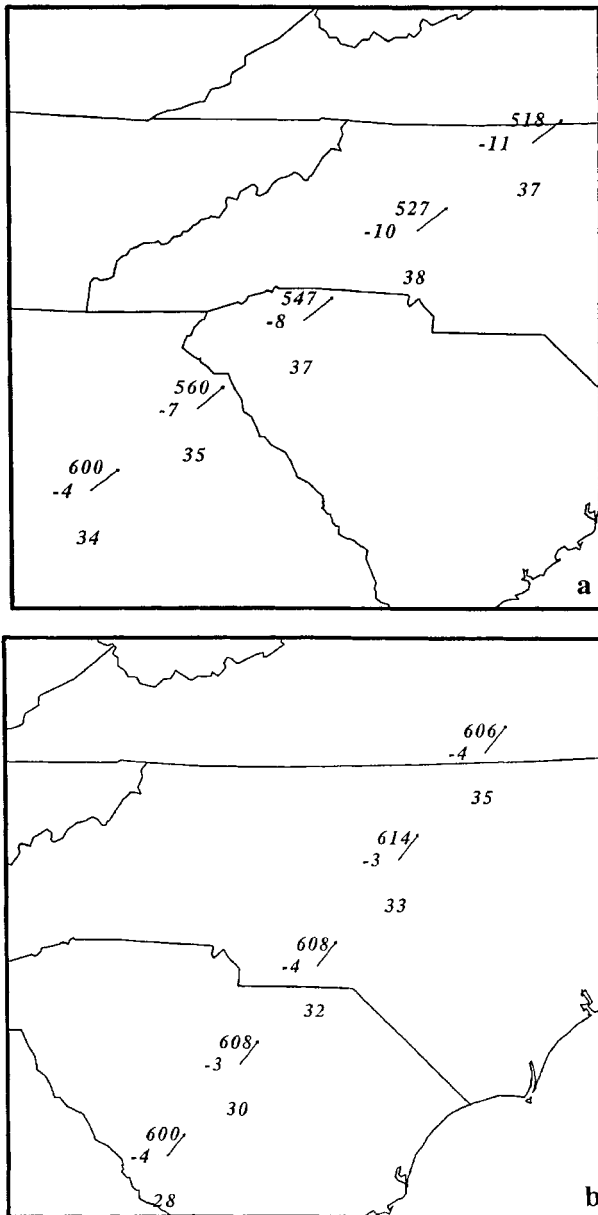


Fig. 9. Trajectories constructed from the 12 km MASS simulation. Station plots contain pressure (hPa), temperature (C), and total wind speed (ms^{-1}). Displayed wind vectors depict total wind. Parcels initialized at **a** 1200 UTC and ended 1400 UTC 25 January 1990, and **b** 1800 UTC and ended 2200 UTC 25 January 1990

Rossby numbers average 0.1, again indicating balanced flow. The mid-level jet is balanced with weak mid-level descent over the Piedmont.

4.3 Mid-level jet development and convection

We also examine the relationship between convection (release of latent heat) and jetlet

development. In the event case, the unbalanced, accelerating, mid-level jetlet exit region has a thermally direct circulation with ascent in the right exit region. Convection locally warms the area due to latent heating increasing the thermal gradient and the PGF, in turn, accelerating the jet (Hamilton et al., 1998).

Figure 10 depicts the mid-level jetlet and accumulated convective precipitation (over 1/2 h) of the event case. The convection tends to develop toward the right exit region. At 0200 UTC 28 November 1988, convection is associated with the accelerating jetlet in the right exit region of the jetlet core (area shaded $> 40 \text{ ms}^{-1}$) and an area of warm air is also associated with it. By 0600 UTC 28 November 1988, the jetlet develops into a large mid-level jet with a thermally direct circulation with strong ascent and an elongated area of convection in the right exit region.

Another MASS simulation with convection deactivated is performed to examine the relationship of latent heating to mid-level jet development. In the “no latent heat” simulation, the mid-level jet is present over GA, SC and NC at 0600 UTC 28 November 1988 (Fig. 11a); the simulation with latent heating is depicted in Fig. 11b. The mid-level jet over NC is similar between the simulations. Over the Piedmont, the wind is $\sim 2 \text{ ms}^{-1}$ less in the simulation without latent heating. Due to the warm Mexican air mass over the Piedmont, the environment is predisposed to develop a strong mid-level jet. However, latent heating from convection does increase the magnitude of the mid-level jet.

Parcel trajectories are constructed for the “no latent heating” simulations. Figure 12 depicts a parcel trajectory derived from a MASS simulation suppressing the release of latent heat. Over western NC, the wind speed is $\sim 5 \text{ ms}^{-1}$ slower in the run without latent heating. The Lagrangian Rossby numbers (Table 3) are less than 0.5, which indicates a balanced flow. While the environment is conducive to mid-level jet development, it appears the latent heat energy, in part, enhances the development of a mid-level unbalanced jetlet. The PGF is roughly twice as strong in the event case with latent heating. The stronger PGF (with latent heating) continues to accelerate the jet in what normally would be the exit region, which then creates an unbalanced jet with a thermally direct ageostrophic circulation. In addition, this

Table 2. Same as Table 1 except trajectory is initiated at 1200 UTC 25 January 1990 and ending 1600 UTC 25 January 1990

| Time (UTC) | LAT (°N) | LON (°W) | PRS (hPa) | CO $\times 10^{-3} \text{ms}^{-2}$ speed/dir | PGF $\times 10^{-3} \text{ms}^{-2}$ speed/dir | NBE Total $\times 10^{-8} \text{s}^{-1}$ | V_{total} (ms^{-1}) speed/dir | Ro_L | OMGA 10^{-1}Pa s^{-1} | Div ($\times 10^{-5}$) |
|---------------|-------------|-------------|--------------|--|---|--|---|--------|------------------------------------|-----------------------------|
| 25/1200 | 33.50 | 84.25 | 600 | 2.7/323 | 3.73/145 | -9.886 | 33.6/233 | *** | -6.229 | 1.093 |
| 25/1230 | 33.84 | 83.73 | 584 | 2.76/322 | 2.44/137 | 1.465 | 34/231 | 0.117 | -14.678 | 6.743 |
| 25/1300 | 34.20 | 83.2 | 560 | 2.88/319 | 4.5/192 | 1.431 | 35.1/229 | 0.291 | -8.14 | 2.893 |
| 25/1330 | 34.57 | 82.67 | 550 | 2.99/320 | 3.43/158 | 4.435 | 36.1/230 | 0.089 | -5.452 | 1.532 |
| 25/1400 | 34.95 | 82.11 | 547 | 3.07/321 | 3.27/150 | -5.25 | 36.7/231 | 0.196 | -3.654 | 3.168 |
| 25/1430 | 35.32 | 81.54 | 537 | 3.14/322 | 2.34/122 | 2.227 | 37.3/232 | 0.370 | -4.803 | 1.442 |
| 25/1500 | 35.68 | 80.95 | 527 | 3.21/323 | 2.35/122 | 3.814 | 37.8/233 | 0.450 | -2.701 | 1.762 |
| 25/1530 | 36.05 | 80.35 | 519 | 3.23/323 | 2.99/134 | 4.750 | 37.6/234 | 0.416 | -1.178 | -0.967 |
| 25/1600 | 36.40 | 79.75 | 518 | 3.19/324 | 2.88/138 | 3.903 | 36.9/236 | 0.364 | -1.058 | -2.067 |

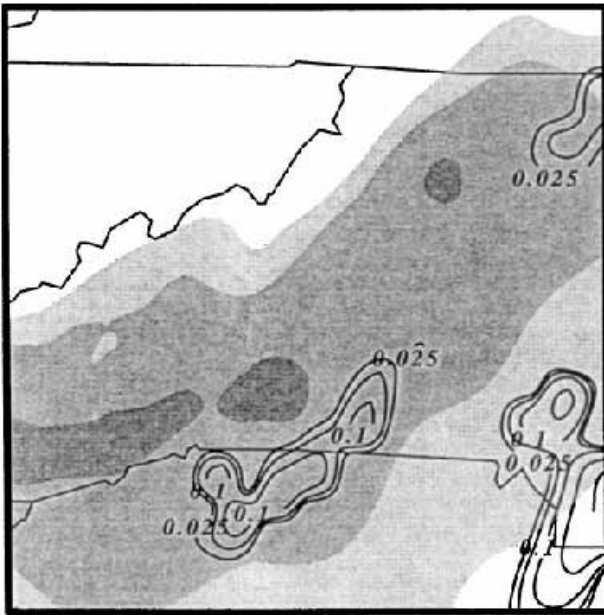


Fig. 10. MASS simulated, 12 km mesh, 600 hPa, wind isotachs (shaded at intervals of 5 for speeds greater than 35ms^{-1}) and convective precipitation (solid lines, contoured at 0.025, 0.05, 0.1 and 0.15, mm/0.5h) valid at 0200 UTC 26 November 1988

ascent is over the warm air, which helps to destabilize the environment. As this jetlet develops and propagates eastward, the thermally direct ageostrophic circulation merges with an area of ascent between the PJ and the STJ creating an area of strong ascent over the Piedmont.

In the non-event case, the main area of convection generally occurs in the left exit region of the jet (not shown), which is opposite of the event case. The balanced jet exit region has an associated thermally indirect circulation

with ascent in the left exit region. At 1400–2100 UTC 25 January 1990, the jet continues to develop. At 1800 UTC 25 January 1990, there is no convection, which suggests weak dynamics about this jet (Fig. 13a). By 0000 UTC 26 January 1990, the right entrance region (ascent) of the mid-level jet is over eastern TN, which creates an area of light convective precipitation over western NC (Fig. 13b). Another MASS simulation is performed with no convection to examine the relationship to jetlet development. In the non-event “no latent heat” simulation, the mid-level jet develops farther to the west associated with the balanced QG system over the TN valley. While the convection areas are disconnected from the ageostrophic circulations about the jet, it appears that the latent heat release from convection does modify the mid-level jet (on a meso- α scale).

We also compare the mid-level jets at the event time (0600 UTC 28 November 1988, Fig. 14) and non-event time (Fig. 13a – 1800 UTC 25, and Fig. 13b – 0000 UTC 26 January 1990) and found several differences. Comparing Fig. 14 to Fig. 13a we find the right side of the jetlet is over central NC (event case) while in the non-event case the jetlet is moving into central VA. There is a line of convective precipitation along the right side of the jetlet and over central NC in the event case, while the non-event case does not have any convective precipitation near the jetlet or central NC. We also compare Fig. 14 to Fig. 13b. The right side of the jet is over central NC in both the event and non-event case. The location of the convective precipitation relative to the jetlet is very different. In the event case, there is a

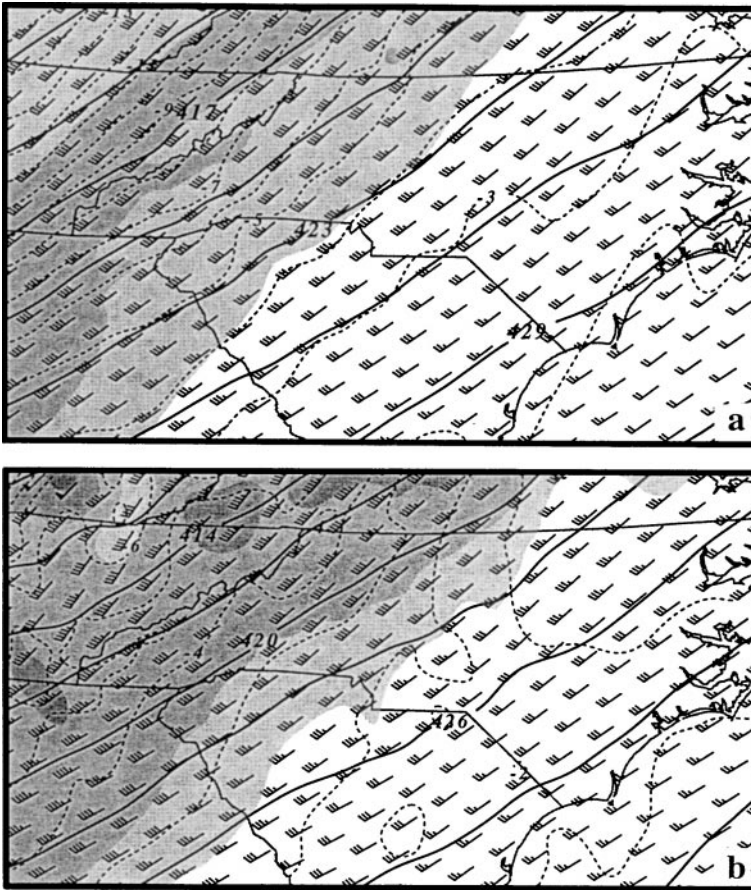


Fig. 11. MASS simulated, 12 km mesh, 600 hPa, wind isotachs and vectors (shaded at intervals of 5 for speeds greater than 35 ms^{-1}), temperature (dashed lines, C), and height (solid lines, dm) valid at 0600 UTC 28 November 1988 **a** without latent heating, and **b** with latent heating

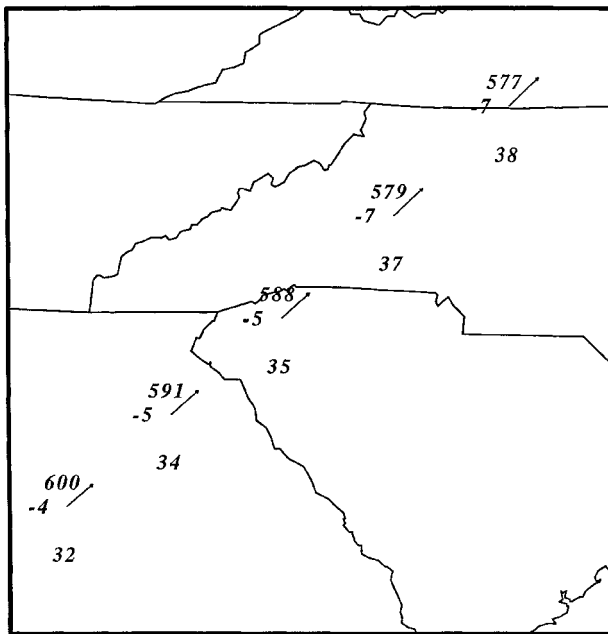


Fig. 12. Trajectory constructed from the 12 km MASS simulation without latent heating. Station plots contain pressure (hPa), temperature (C), and total wind speed (ms^{-1}). Displayed wind vectors depict total wind. Parcels are initialized at 0000 UTC and ended 0400 UTC 28 November 1988

line of convective precipitation along the right side of the jetlet and over central NC; in the non-event case, convective precipitation is much less intense and located beneath the mid-level jet over western NC.

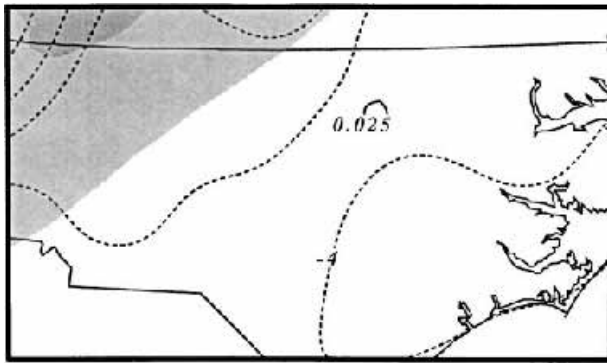
In summary, the event case warm pool, i.e., air from MX and warmed by latent heating, helps maintain the height gradient and the PGF. This, in turn, accelerates the jet in what normally would be the jet exit region and induces a thermally direct circulation. In the non-event case, the thermal gradient is much weaker and not as well organized.

5. Potential vorticity

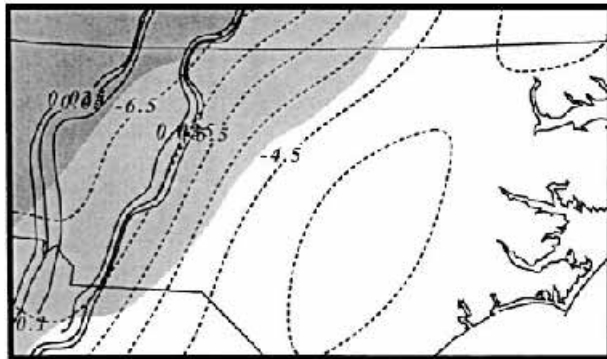
Parts I and II detail the 3-day evolution of the low-level PV maximum. In the event case, the PV maximum originated in the upper-levels over central MX, is tracable from central MX, along the Gulf Coast and over central NC at the time of the tornado. The PV is primarily maintained by the tilting of the horizontal component of vorticity into the vertical through horizontally varying

Table 3. Forward trajectory initiated at 0000 UTC 28 November 1988, originating at the same location as previous parcel and ending at 0400 UTC 28 November 1988. Trajectory data is derived from 24 km MASS simulation without latent heating. The following abbreviations are defined: Latitude (LAT), Longitude (LON), Pressure (PRS), Temperature (TMP), Total wind (V_T), Pressure gradient force vector (PGF), Coriolis force vector (COR) and Lagrangian Rossby number (Ro_L)

| Time (UTC) | LAT (°N) | LON (°W) | PRS (hPa) | TMP (°) | V_{total} (ms^{-1}) speed/dir | PGF $\times 10^{-3} ms^{-1}$ | COR $\times 10^{-3} ms^{-2}$ | Ro_L |
|------------|----------|----------|-----------|---------|--|------------------------------|------------------------------|--------|
| 28/0000 | 33.5 | 84.5 | 600 | -4.04 | 32.3/228 | 2.92/149 | 2.6/319 | * * * |
| 28/0100 | 34.21 | 83.53 | 591 | -5.14 | 34/228 | 2.63/151 | 2.79/318 | 0.455 |
| 28/0200 | 34.96 | 82.51 | 588 | -5.38 | 35.3/228 | 4.63/154 | 2.95/318 | 0.256 |
| 28/0300 | 35.75 | 81.45 | 579 | -6.72 | 37.1/228 | 2.63/143 | 3.16/318 | 0.266 |
| 28/0400 | 36.57 | 80.33 | 577 | -6.79 | 38.3/228 | 3.73/128 | 3.32/318 | 0.084 |



a



b

Fig. 13. MASS simulated, 12 km mesh, 600 hPa, wind isotachs (shaded at intervals of 5 for speeds greater than $35 ms^{-1}$), surface convective precipitation (solid lines, contoured 0.025, 0.05, and 0.1, mm/0.5h) and temperature (dashed lines, C) valid at **a** 1800 UTC 25, and **b** 0000 UTC 26 January 1990

diabatic heating. The non-event case, in contrast, does not have a long-lasting tracable low-level PV maximum.

The evolutions of the PV maxima are investigated for the last 6 hours and are related to surface cyclogenesis for both cases. In the event case,

Figs. 15a, b and c depict the surface pressure and PV over the 925 to 875 hPa layer valid 0200, 0400 and 0600 UTC 28 November 1988. These figures highlight the relationship between low-level PV and surface cyclogenesis. The 900 hPa PV maxima are located just to the west of the surface trough and are associated with the areas of maximum trough deepening. At 0000 UTC there is a PV maximum (>5 PV units) over northeastern GA and by 0200 (Fig. 15a) the PV maximum propagates over western SC and is associated with a mesocyclone (<1002 hPa). By 0400 UTC (Fig. 15b), the PV maximum is near Charlotte, NC (CLT) and is associated with the 1000.5 hPa isobar. By 0600 UTC (Fig. 15c), the PV maximum (>4.5 PV units) moves over to central NC at the time of the tornado outbreak and is associated with a 995.5 hPa isobar.

Figures. 16a, b, c and d depict the relationship between the surface pressure and PV over the 925 to 875 hPa layer valid 1500, 1800, 2100 UTC 25 and 0000 UTC 26 January 1990 for the non-event case. At 1500 UTC (Fig. 16a), there are isolated PV maxima associated with the surface trough. By 1800 UTC (Fig. 16b), the low-level PV (>2 units) is still associated with the surface trough. However, most of the PV is over GA and far western NC. By 2100 UTC (Fig. 16c), the low-level PV maxima over GA is weakening and the maximum over western NC is moving northeast. By 0000 UTC (Fig. 16d), the low-level PV maximum is moving over southern VA. The surface front over the Piedmont does not have any associated low-level PV.

We examine vertical cross sections which bisect the low-level PV maximum and the upper-level jet streaks. Figure 17a depicts θ_c and PV along the northwest to southeast cross

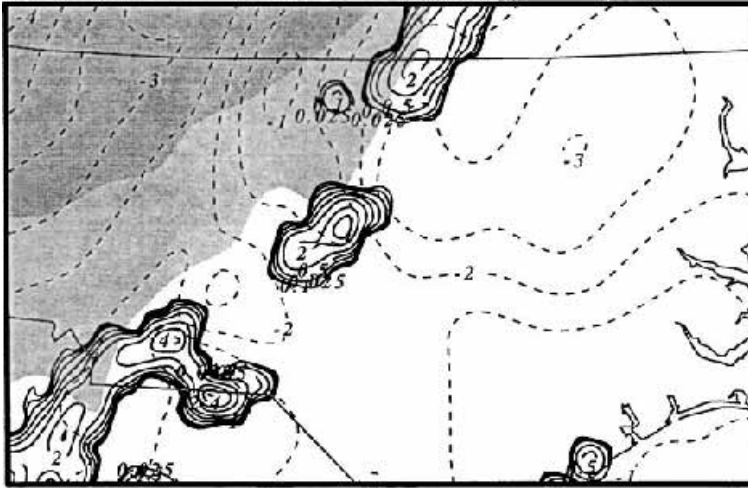


Fig. 14. MASS simulated, 12 km mesh, 600 hPa, wind isotachs (shaded at intervals of 5 for speeds greater than 35 ms^{-1}), temperature (dashed lines, C), and surface convective precipitation (solid lines, contoured 0.01, 0.025, 0.05, 0.1, 0.2, 0.3 and 0.4, mm/0.5h) valid at 0600 UTC 28 November 1988

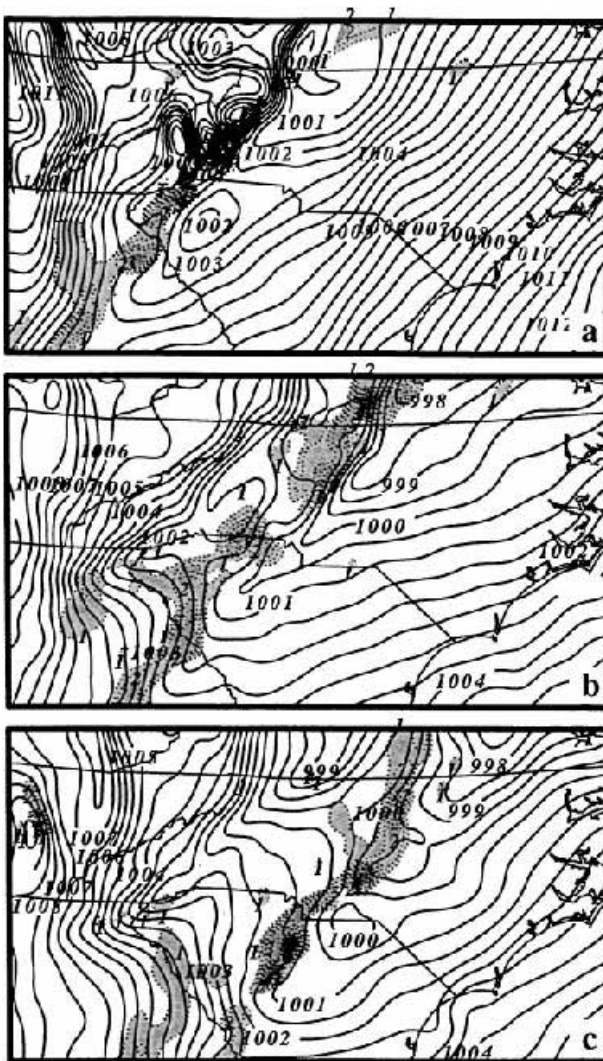


Fig. 15. MASS simulated, 12 km mesh, 900 hPa PV (shaded greater than 1 by 0.5 PV units) and mean sea-level pressure (solid lines, hPa) valid at **a** 0200 UTC, **b** 0400 UTC, and **c** 0600 UTC 28 November 1988

sections centered over northern SC for 0400 UTC 28 November 1988. At 0600 UTC (Fig. 17b), the cross section is centered over RDU. These cross sections depict the strongest PV in the low-levels. Hourly cross sections (not shown) bisecting the low-level PV maximum indicate that the PV is a low-level feature. Just as in the preceding 48 hours, event case PV is transported and/or generated in the low-levels.

The non-event cross section (Fig. 18a) valid 1800 UTC 25 January 1990 extends from IL, over the Piedmont to the Atlantic Ocean (east of Cape Hatteras). The cross section depicts the PV transport from the left flank of the PJ entrance region down to the low-levels west of the Piedmont. This supports the concept that PV is transported downward by a tropopause fold (Danielsen, 1968). At 2100 and 0000 UTC (Figs. 18b and c), the cross sections depict downward transport of PV but the eastward extent of the PV only reaches western NC. The low-level PV maxima over the Piedmont are weak, sporadic and associated with convection not with the downward transport of PV. There is no interaction between upper- and lower-level disturbances characterized by non uniform PV which would result in a significant increase in relative vorticity at the surface (Zehnder and Keyser, 1991).

We also examine the relationship between convective precipitation (diabatic energy source) and PV generation. The 900 hPa event case PV and the latent heating are generally associated with convection. The low-level PV maxima increase, in part, from latent heat energy associated with convection. The 0635 UTC radar

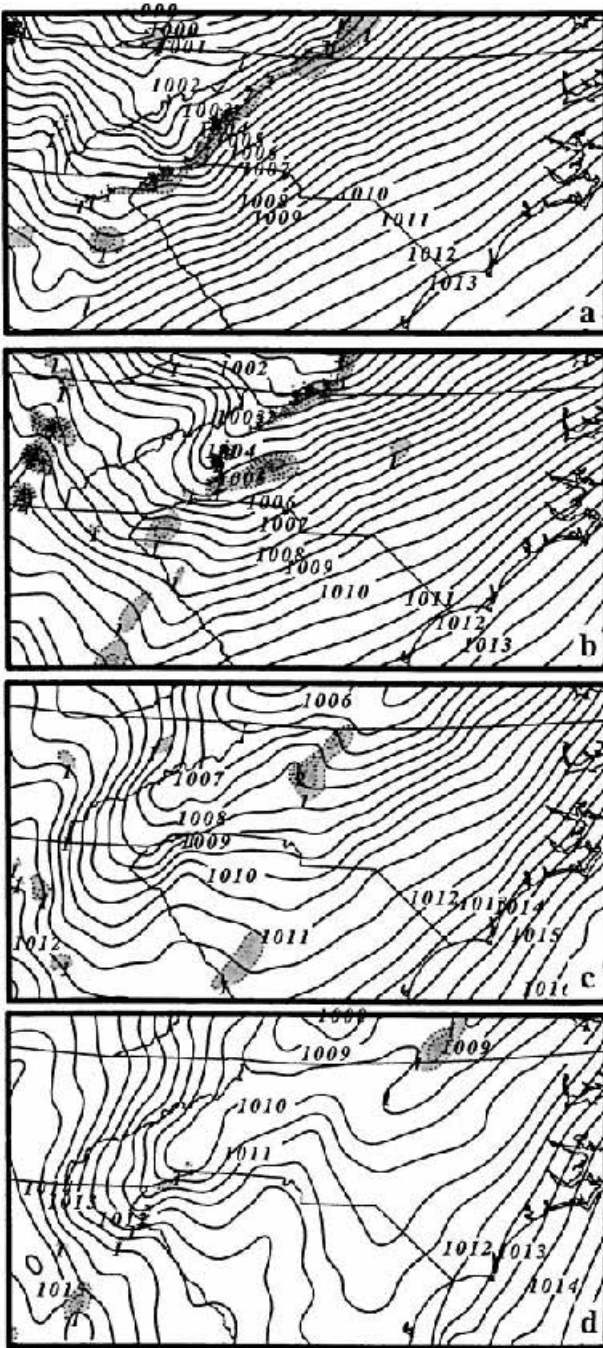


Fig. 16. MASS simulated, 12 km mesh, 900 hPa PV (shaded greater than 1 by 0.5 PV units) and mean sea-level pressure (solid lines, hPa) valid at **a** 1500 UTC 25, **b** 1800 UTC 25, **c** 2100 UTC 25, and **d** 0000 UTC 26 January 1990

summary (Fig. 19a) agrees well with the model simulated convection at 0600 UTC (Fig. 19b). Also, the low-level PV is associated with the diabatic convective heating rates (Fig. 19c).

The simulated 1800 UTC convection for the non-event case (Fig. 20b) agrees with the 1735 UTC radar summary (Fig. 20a). Convection is over western NC and SC, central GA, and eastern NC with a dry area over the Piedmont. The low-level PV (Fig. 20c) along the Appalachians is associated with the convection and latent heating. This PV, convection and latent heating is maintained at 2100 UTC 25 and 0000 UTC 26 January 1990 (not shown).

Potential vorticity can be increased locally either by transport or generation. The generation of PV, through diabatic processes, may be examined using the Lagrangian PV equation (Eq. 1) (Gidel and Shapiro, 1979) and may be estimated by:

$$\begin{aligned} \frac{d}{dt} \left[-(\zeta_\theta + f) \frac{\partial \theta}{\partial p} \right] &= \underbrace{- (\zeta_\theta + f) \frac{\partial}{\partial p} \left(\frac{d\theta}{dt} \right)}_1 - \underbrace{\left(\frac{\partial \theta}{\partial p} \right) \hat{k} \cdot \nabla_\theta \times \vec{F}}_2 \\ &+ \underbrace{\left(\frac{\partial \theta}{\partial p} \right) \hat{k} \cdot \nabla_\theta \left(\frac{d\theta}{dt} \right) \times \frac{\partial \vec{V}}{\partial \theta}}_3. \end{aligned} \quad (1)$$

Term 1 relates to the production or destruction of PV to vertical gradients of diabatic heating with isentropic absolute vorticity. Term 2 represents the change in PV resulting from horizontal gradients of diabatic heating within regions of horizontally varying frictional stresses. Term 3 represents the change in PV resulting from the tilting of the horizontal component of vorticity into the vertical through horizontally varying diabatic heating. The relative contribution of each term in the PV Eq. (1) is evaluated in a manner analogous to Kaplan and Karyampudi (1992b) using parcel trajectory data with the exception of the gradient field, which is calculated using a centered finite differencing scheme about the center trajectory point.

Using trajectories, we examine the PV maximum over central NC at the time of the tornado (Table 4). Figure 21a depicts the parcel trajectory and the latent heating due to convection at 0600 UTC. There is a maximum ($>5 \text{ C h}^{-1}$) over central NC. The parcel's PV increases to 3.647 PV units as it passes through the convection (latent heating). The diabatic heating produces

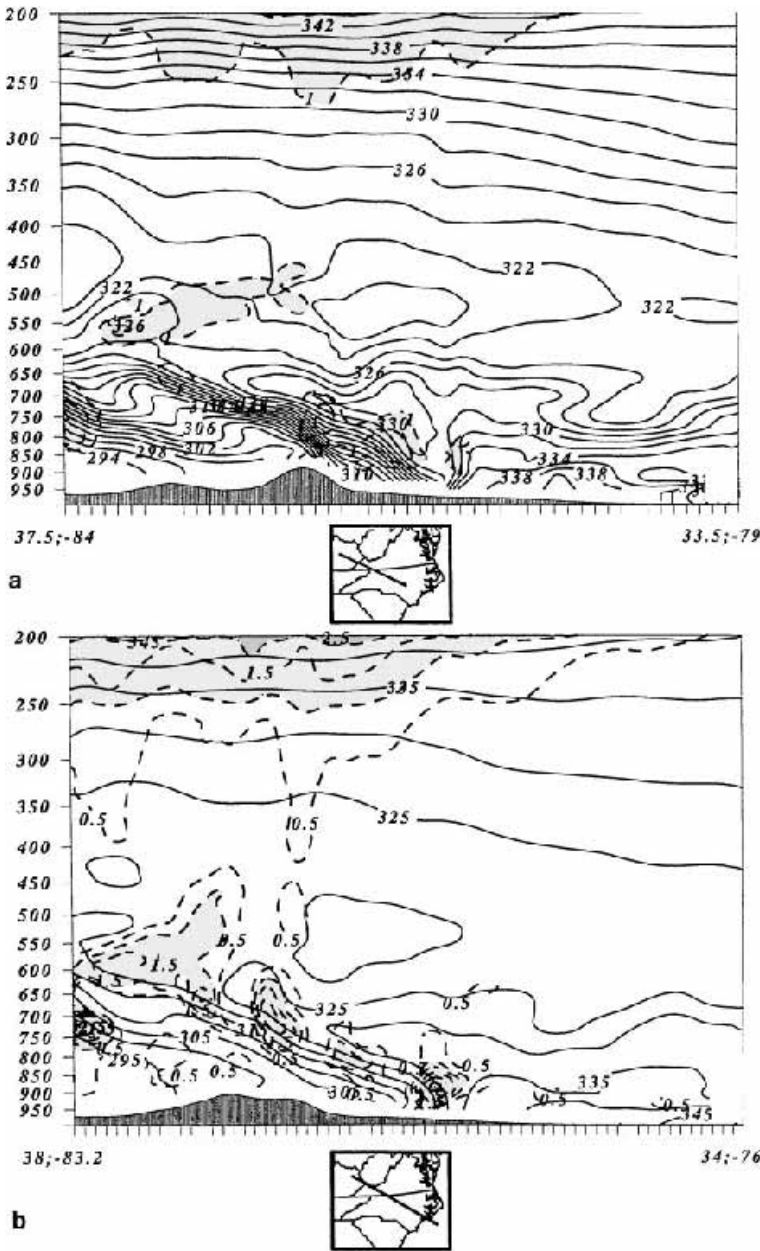


Fig. 17. MASS simulated, 12 km mesh, cross sections of θ_e (solid lines, K) and PV (contoured by 0.5 and shaded greater than 1 PV units); **a** from (37.5N, 84W) to (33.5N, 79W) valid at 0400 UTC 28 November 1988, and **b** from (38N, 83.2W) to (34N, 76W) valid at 0600 UTC 28 November 1988

PV so we evaluated the relative contribution of each term in Eq. (1). Term 1 contributes 32% to the production of PV by the change in static stability. Term 2 contributes 19% to the change in PV resulting from horizontal gradients of diabatic heating within regions of friction. Term 3 contributes 49% to the production of PV resulting from the tilting of the horizontal component of vorticity into vertical through horizontally varying diabatic heating.

We also examine the PV maximum over central NC at the expected time of the non-event (Table 5). Figure 21b depicts the parcel trajectory

and convection (latent heating) at 1200 UTC. There is no latent heating $>1 \text{ C h}^{-1}$ over eastern GA or western NC and SC so the parcel's PV increase is small (0.471 PV units) as it moves over central NC. We evaluate the relative contribution of each term in the PV Eq. (1). Term 1 produces a small amount of anticyclonic PV while term 2 (friction) and term 3 (tilting) produce cyclonic PV. At 0000 UTC 26, the only area of low-level PV is well north of RDU (over central VA) so the data is not included.

We conclude that the PV maxima in the event case increases over central NC through the tilting

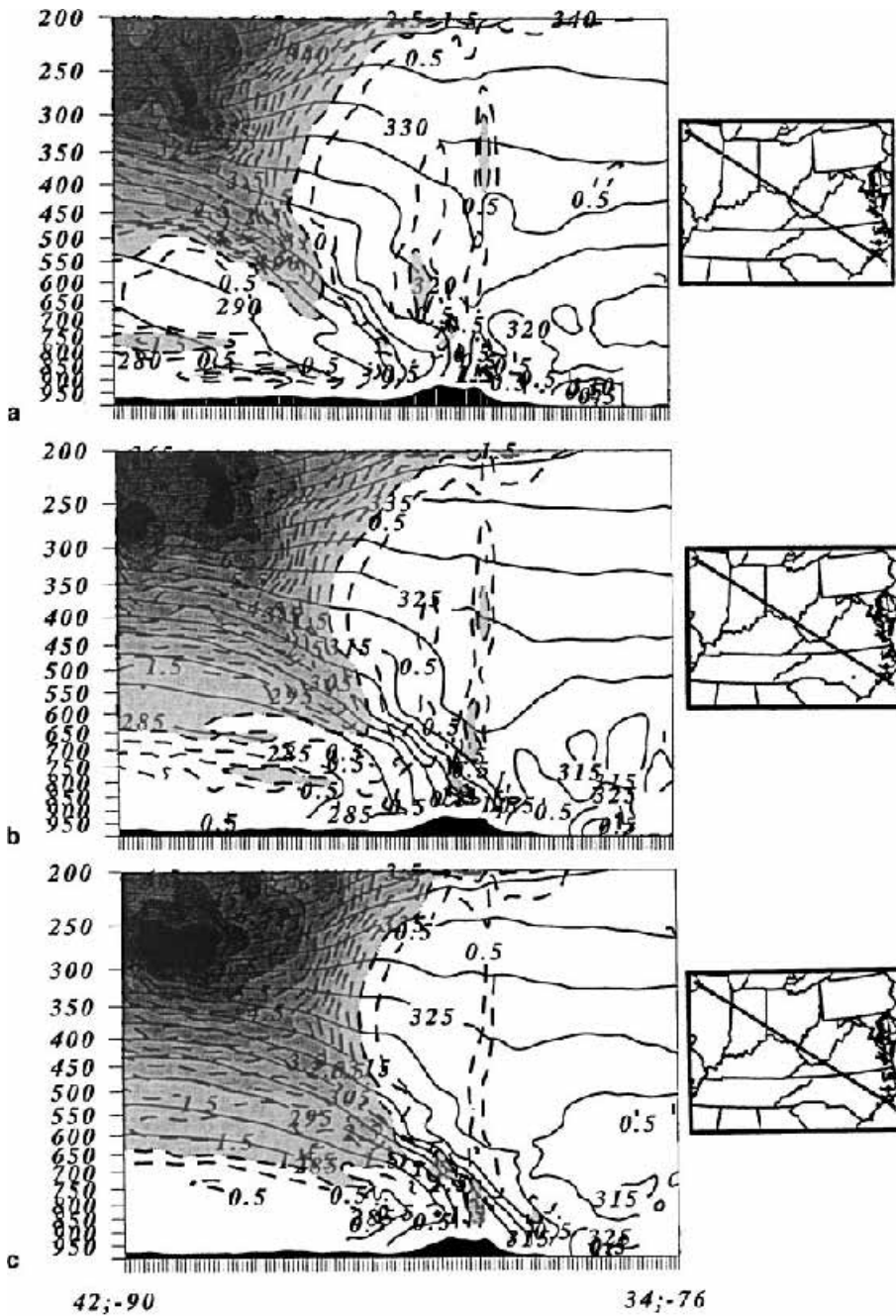


Fig. 18. MASS simulated, 12 km mesh, cross section from 42N, 90W to 34N, 76W. Including, θ_e (solid lines, K) and PV (contoured by 0.5 and shaded greater than 1 PV units) valid at **a** 1800 UTC 25, **b** 2100 UTC 25, and **c** 0000 UTC 26 January 1990

term associated with diabatic forcing. In the non-event, there is little change in the low-level PV over central NC.

6. Low-level environment favorable for severe weather

We examine the low-level stability over the Piedmont using the lifted index (LI) (Bluestein, 1993). For the event case, at 0600 UTC 28

November 1988 the LI pattern (Fig. 22a) depicts large negative LI over the eastern Piedmont, which is associated with the warm Mexican airmass above the warm moist air from the Carolina coast, indicating strong potential for severe weather. The non-event case LI field (Fig. 22b) at 1800 UTC 25, January 1990 depicts positive LI values over the Piedmont, which indicates little chance for severe weather. By 0000 UTC 26 January 1990 (Fig. 22c), the LI

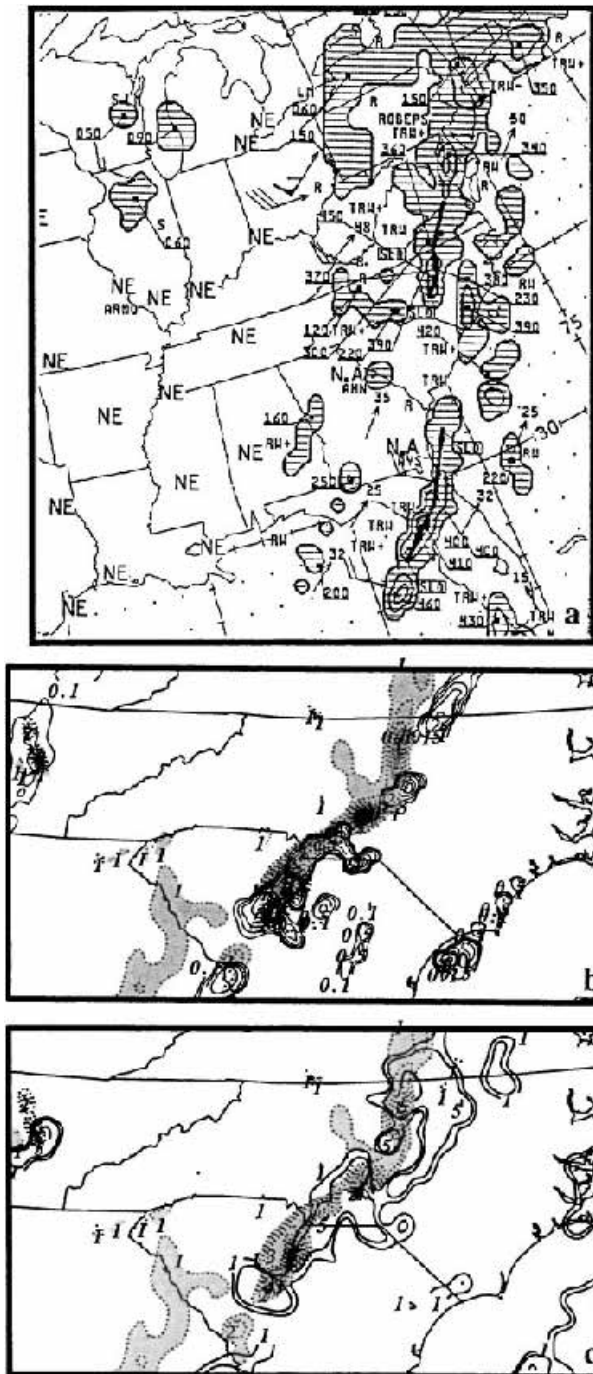


Fig. 19. **a** NWS radar summary for 0635 UTC 28 November 1988, **b** MASS simulated, 12 km mesh, 900 hPa PV (contoured by 0.5 and shaded greater than 1 PV units) and surface convective precipitation (contoured 0.1, 0.5, 0.1, 0.2, 0.3, 0.4 and 0.5, mm/0.5h), and **c** 900 hPa PV (contoured by 0.5 and shaded greater than 1 PV units) and latent heating (contoured at 1, 2 and 5 °C h⁻¹) valid at 0600 UTC 28 November 1988

over the Piedmont indicates an even more stable airmass. *Note that at the time of the event and non-event, the forecasters did not have access to*

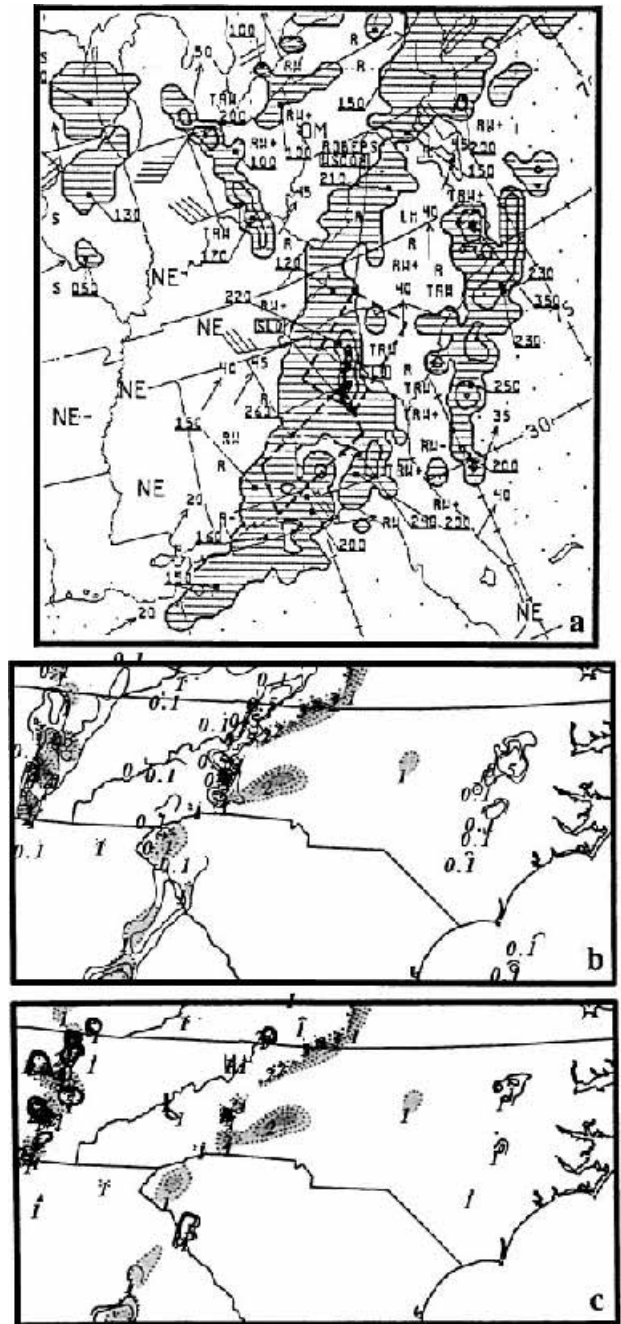


Fig. 20. **a** NWS radar summary for 1735 UTC 25 January 1990, **b** MASS simulated, 12 km mesh, 900 hPa PV (contoured by 0.5 and shaded greater than 1 PV units) and surface convective precipitation (contoured 0.1, 0.5, 0.1, 0.2, 0.3, 0.4 and 0.5, mm/0.5h), and **c** 900 hPa PV (contoured by 0.5 and shaded greater than 1 PV units) and latent heating (contoured at 1, 2 and 5 °C h⁻¹) valid at 1800 UTC 25 January 1990

the high-resolution model data. The RDU forecasters calculated the lifted index from the Greensboro, NC sounding, which yielded a value

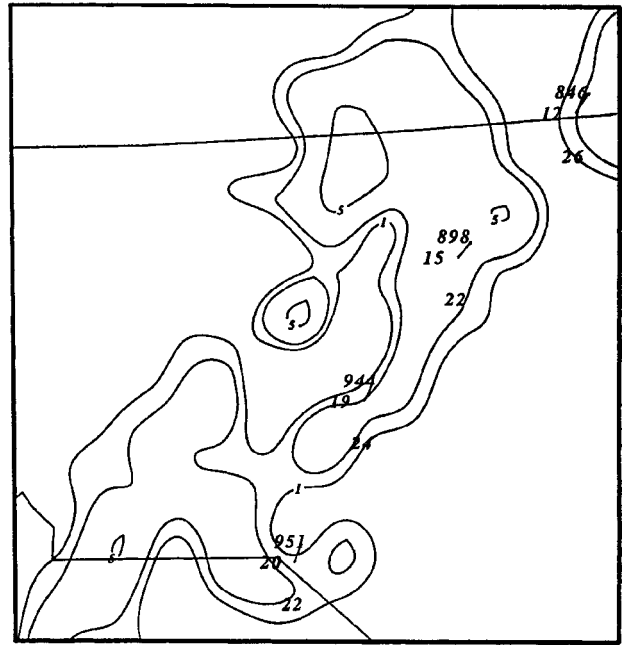
Table 4. Trajectory initialized at 0400 UTC 28 November 1988, passed over RDU at 0600 UTC and ended at 0700 UTC 28 November 1988. Trajectory data are hourly and were derived from a 24 km MASS simulation. The following abbreviations are defined: Latitude (LAT), Longitude (LON), Pressure (PRS), Temperature (TMP) and Potential vorticity (PV)

| Time (UTC) | LAT (°N) | LON (°W) | PRS (hPa) | TMP (°C) | PV (PV units) |
|------------|----------|----------|-----------|----------|---------------|
| 0400/28 | 35.0 | 79.6 | 951 | 19.98 | 1.302 |
| 0500/28 | 35.7 | 79.17 | 944 | 19.45 | 2.906 |
| 0600/28 | 36.3 | 78.7 | 898 | 14.70 | 3.647 |
| 0700/28 | 36.9 | 78.0 | 846 | 11.68 | 2.092 |

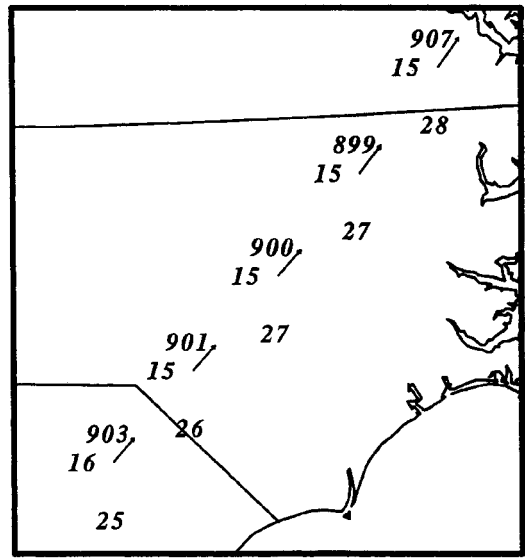
of 1 for the event case and 2 for the non-event case.

The fact that the mesoscale environment of the event case is much more conducive for a severe weather outbreak compared with the non-event, is also reflected in the radar summaries at 0635 UTC 28 November 1988 (Fig. 19a) and 1735 UTC 25 January 1990 (Fig 20a). In the event case, a solid line of heavy thunderstorms is over central NC with maximum tops of nearly 15 km. There are additional thunderstorms over western NC and the NC coastal region. In the non-event case there are no thunderstorms over central or western NC. There are rainshowers over western NC with maximum tops of 6.5 km and thunderstorms over the NC coast with maximum tops of 8.4 km. Also, we compare the radar summaries at 0635 UTC 28 November 1988 (Fig. 19a) and 2335 UTC 25 January 1990 (not shown). In the event case, a solid line of heavy thunderstorms is over central North Carolina with maximum tops of nearly 15 km while the non-event case has no thunderstorms. In summary, the event case has more clusters of cumulonimbus clouds with a much greater depth, which indicates a stronger convective instability.

We also examine the mid-level jet streaks and the low-level total wind velocity shear they create. Figure 23a, b (event case) and Fig. 23c–f (non-event case) depict the magnitude of wind shear between the wind vectors (ms^{-1}) at 925 or 850 and 500 hPa levels. Figure 23a, b is valid at 0600 UTC 28 November 88 (event case). Strong shear (32ms^{-1}) over the 850 and 500 hPa layer propagates over central NC as the low-level easterly flow veers to west-south-west in the mid-



a



b

Fig. 21. MASS simulated, 12 km mesh, trajectory and 900 hPa latent heating (contoured at 1, 2 and 5 C h^{-1}). Station plots contain pressure (hPa), temperature ($^{\circ}\text{C}$), and total wind speed (ms^{-1}). Displayed wind vectors depict total wind **a** from 0400 to 0700 UTC 28 November 1988, and **b** from 1600 to 2000 UTC 25 January 1990

level jet. The shear of the 925–500 hPa layer approaches 40ms^{-1} . The lower layer (850 to 700 hPa) contains ~ 90 percent of the total shear. As the mid-level jet moves over central NC, the low-level vertical shear increases rapidly, which increases the possibility of severe weather.

Table 5. Same as Table 4 except trajectory initiated at 1600 UTC 25 January 1990 and ended at 2000 UTC 25 January 1990

| Time (UTC) | LAT (°N) | LON (°W) | PRS (hPa) | TMP (°C) | PV (PV units) |
|------------|----------|----------|-----------|----------|---------------|
| 1600/25 | 34.3 | 79.9 | 903 | 15.82 | 0.014 |
| 1700/25 | 34.9 | 79.2 | 901 | 15.52 | 0.035 |
| 1800/25 | 36.5 | 78.5 | 900 | 15.43 | 0.122 |
| 1900/25 | 36.2 | 77.7 | 899 | 14.75 | 0.405 |
| 2000/25 | 36.8 | 77.0 | 907 | 14.96 | 0.471 |

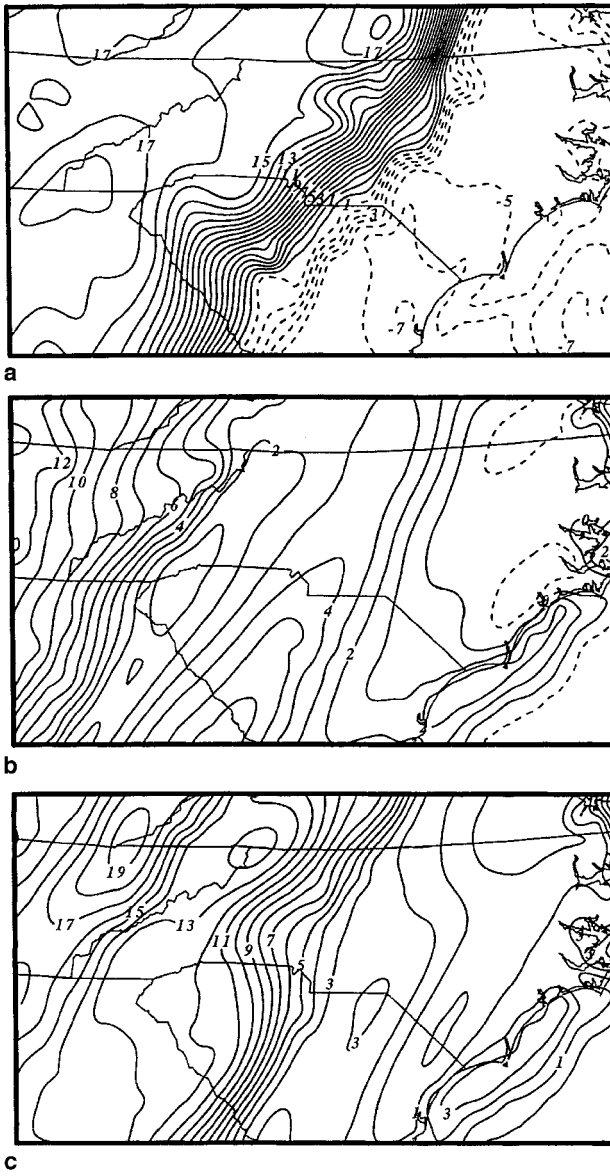


Fig. 22. MASS simulated, 12 km mesh, Lifted Index values (solid lines indicate positive values and dashed lines indicate negative values) valid at **a** 1800 UTC 28 November 1988, **b** 1800 UTC 25, and **c** 0000 UTC 26 January 1990

Figure 23c, d depict the non-event case at 1800 UTC on the 25 January 1990. The amount of vertical shear (over the 850 to 500 hPa layer) over central NC is insignificant. The 925 to 500 hPa layer at 1800 UTC 25 January 1990 has a larger shear quantity but decreases significantly by the following hour (not shown). By 0000 UTC 26 January 1990 (Fig. 23e, f) the low-level shear increases slightly. Also, most of the shear is near the mid-levels (over the 700 to 500 hPa layer). The weaker non-event case vertical shear indicates a lower potential for severe weather than in the event case.

Another way we investigate low-level wind shear is by the thermal wind. In the event case, there is a strong thermal wind (over the 900 to 500 layer) east of the 600 hPa jet and the surface cold air advection over the Piedmont. There is a second thermal wind maximum associated with the polar jet/front structure located over TN. In the non-event case, the strongest thermal wind is associated with the polar jet/front system located over the TN valley. The thermal wind over the 900 to 500 hPa layer, the 600 hPa jet and the surface temperature are depicted for both the event (Fig. 24a–c) and non-event case (Fig. 25a–d). In the event case, there is a strong thermal wind ($30\text{--}35\text{ ms}^{-1}$) on the leading edge of the 35 ms^{-1} isotach; while the non-event case has a thermal wind of only 5 ms^{-1} associated with the 35 ms^{-1} isotach. Also, this imbalance is out over the very warm surface air ($>20\text{ }^{\circ}\text{C}$). In the non-event case, the strong thermal wind ($30\text{--}35\text{ ms}^{-1}$) is farther to the west, associated with the 40 ms^{-1} isotach, which is more representative of a QG balanced system. Also, the strong thermal wind is over moderately warm surface air ($\sim 16\text{ }^{\circ}\text{C}$).

We also calculate the storm relative helicity (SRH) over central NC using model simulated data. SRH is defined by (e.g. Davies-Jones et al., 1990):

$$\text{SRH} = - \int_0^h \hat{k} \cdot (\vec{V} - \vec{c}) \times \frac{d\vec{V}}{dz} dz, \quad (1)$$

where \vec{V} is the wind velocity, c is the storm relative motion and $d\vec{V}/dz$ is the wind shear vector over the layer. For our study, c is inferred from operational radar summaries. For the event case (0635 UTC summary), the storm was moving at 24 ms^{-1} from 225° and for the non-event case (1835 UTC summary) the storm was

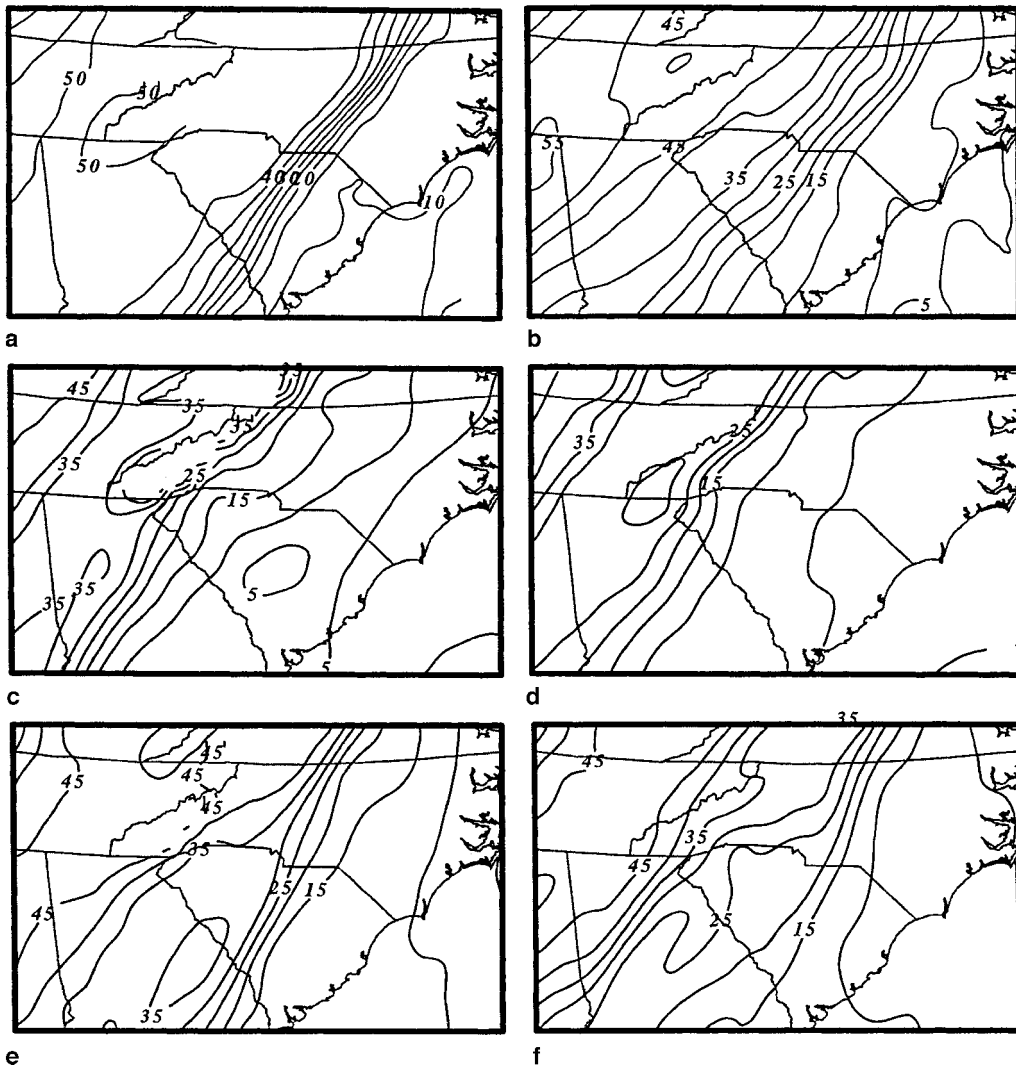


Fig. 23. MASS simulated, 12 km mesh, magnitude of the total wind velocity shear (solid lines, ms^{-1}) between the 925 hPa and the 500 hPa levels valid at **a** 0600 UTC 28 November 1988, **c** 1800 UTC 25 January 1990, and **e** 0000 UTC 26 January 1990; and between the 850 hPa and the 500 hPa levels valid at **b** 0600 UTC 28 November 1988, **d** 1800 UTC 25 January 1990, and **f** 0000 UTC 26 January 1990

moving at 22 ms^{-1} from 215° . At 0600 UTC 28 November 1988 (event case), the maximum value over central NC is $560 \text{ m}^2 \text{ s}^{-2}$. At 1800 UTC 25 (non-event case), the value over central NC was $\sim 240 \text{ m}^2 \text{ s}^{-2}$. By 0000 UTC 26 January 1990, the value over central NC increases to $\sim 300 \text{ m}^2 \text{ s}^{-2}$. The SRH indicates the potential for severe tornadoes for the event case, but not for the non-event case.

7. Divergence profile buoyancy index (DPBI)

The objective of this research is to develop a new way of forecasting severe weather. We incorporate all the features we found to be significant in

our research for the event case study but not for the non-event case study. (1) both the PJ and the STJ are present over the southeast US over the entire 84 hour period. (2) the STJ exit region and the PJ entrance region juxtapose and create strong upper-level divergence over the Piedmont. (3) warm air moves from the Mexican plateau, across the Gulf coast states and over the Carolina Piedmont. (4) the warm MX airmass over the southeast US in conjunction with the cold air advection over the central US produces a strong PGF and creates a robust mid-level jet. (5) the strong low-level imbalance can be measured by strong low-level thermal wind which is out of phase with the mid-level jet and out ahead of

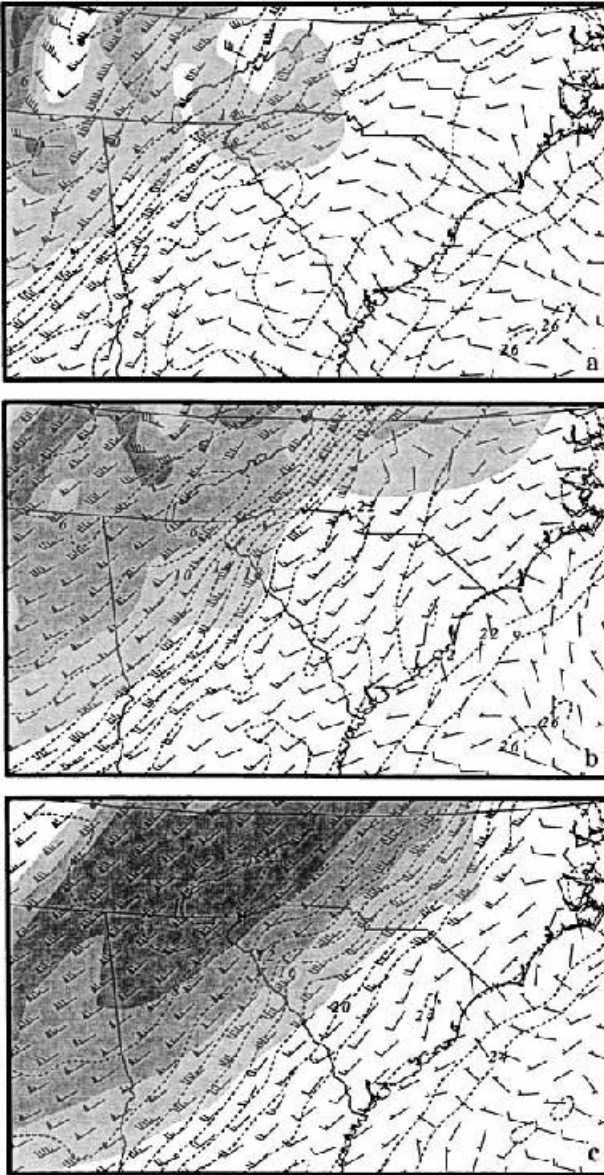


Fig. 24. MASS simulated, 12 km mesh, 600 hPa wind isotachs (shaded at intervals of 5 for speeds greater than 35 ms^{-1}), surface temperature (dashed lines, C), thermal wind barbs over the 900 to 500 hPa layer (ms^{-1}) valid at **a** 0000 UTC, **b** 0300 UTC, and **c** 0600 UTC 28 November 1988

surface cold air advection (front). (6) the mid-level jet right entrance region and its associated thermally direct ageostrophic circulation is associated with a surface trough, surface confluence and convection. All these features interact to maintain themselves as a coherent entity that moves across the Gulf Coast and over the Carolina Piedmont at the time of the tornado outbreak. (7) the movement of the low-level trough (confluence zone) can be traced following

the low-level PV. As the low-level PV propagates along the Gulf Coast and over the Piedmont, diabatic effects (associated with tilting effects) maintain it. We incorporate these features into the DPBI. This index utilizes integrated upper-level divergence, low-level development of a strong baroclinic and shear zone and PV generation associated with low-level tilting effects incorporating shear and thermal gradient, Term 2 of Eq. (2), (Karyampudi et al., 1995):

$$\text{PV} = \underbrace{-\frac{\partial\theta}{\partial p}(\zeta_\theta + f)}_1 \underbrace{-\hat{k} \cdot \frac{\partial\vec{V}}{\partial p} \times \nabla_p\theta}_2. \quad (2)$$

A strong thermal gradient and low-level wind shear develops over the Piedmont. These two factors become extremely large in the low-levels along the baroclinic zone. As air parcels encounter this boundary, they are tilted, generate vorticity and ascend rapidly. Thus, Term 2 (Eq. (4)) is key for the low-level initiation of severe weather. Also, the strong upper-level divergence (Term 1, Eq. (4)) removes mass, which stretches the air column, generating vorticity and maintaining the surface anomaly. Term 1 (Eq. (4)) is calculated by adding the divergence at every 25 hPa over the 375 to 200 hPa layer. Term 2 (Eq. (4)) wind shear is calculated over the 925–875 hPa layer and the thermal gradient is calculated on the 900 hPa level. Finally, the buoyancy of the airmass is incorporated into the index by including the LI, shown below:

$$\text{LI} = T_{500} - T_{\text{Parcel}} \quad (3)$$

Where T_{500} is the 500 hPa temperature (C) and T_{Parcel} is the 500 hPa temperature (C) of a lifted parcel with the average pressure, temperature and dewpoint of the layer in the lowest 100 hPa above the surface. The DPBI is shown below:

$$\text{DPBI} = \underbrace{\left(\sum_{375}^{200} \nabla \cdot \vec{V} \right)}_1 \underbrace{\left[-\hat{k} \cdot \left(\frac{\partial\vec{V}}{\partial p} \times \nabla\theta \right) \right]}_2 \underbrace{(-\text{LI})}_3 \quad (4)$$

Our investigation encompasses the previous 48 hours over the southeastern US. We found that

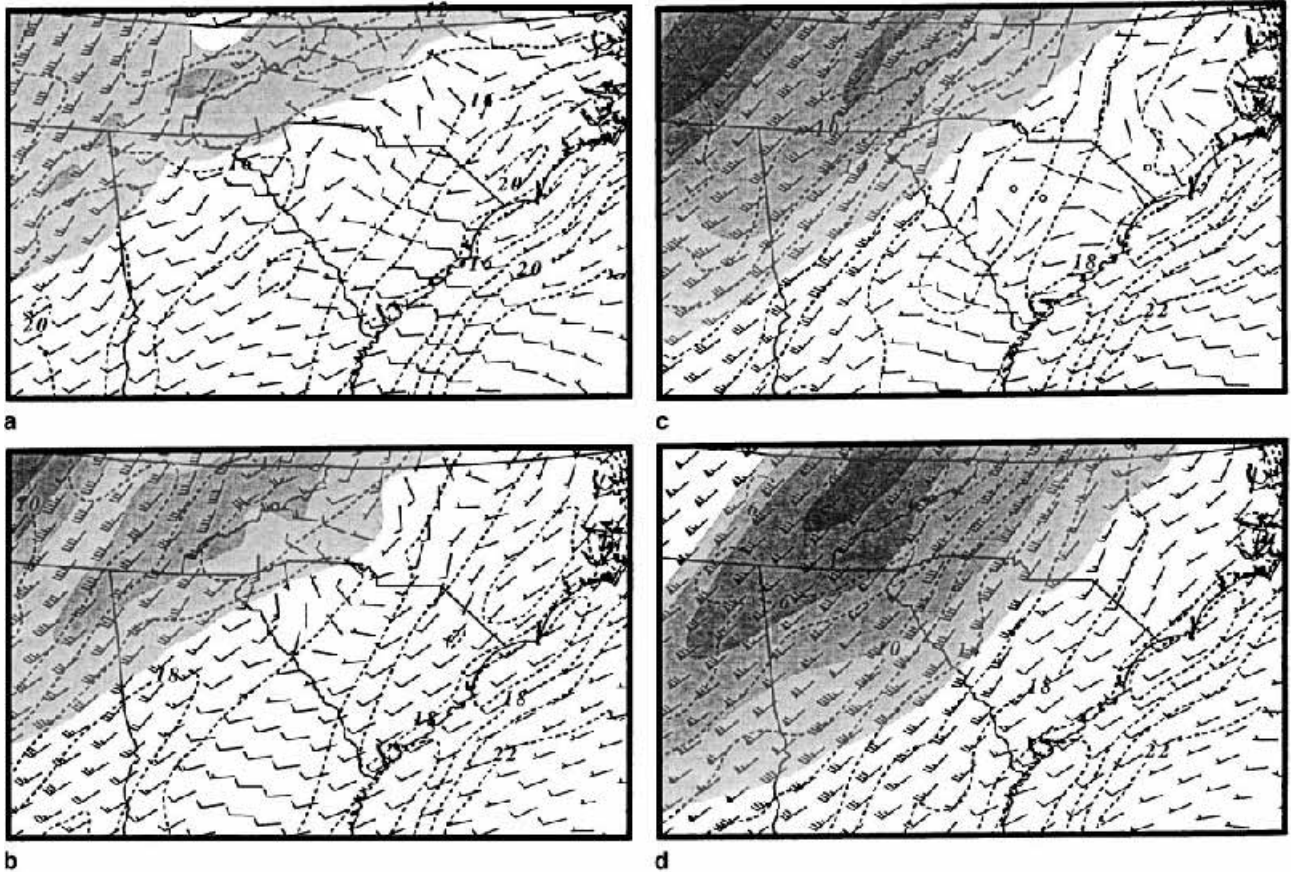


Fig. 25. MASS simulated, 12 km mesh, 600 hPa wind isotachs (shaded at intervals of 5 for speeds greater than 35 ms^{-1}), surface temperature (dashed lines, C), thermal wind barbs over the 900 to 500 hPa layer (ms^{-1}) valid at **a** 1200 UTC, **b** 1500 UTC, **c** 1800 UTC 25, and **d** 0000 UTC 26 January 1990

values over 15 correspond to tornadic activity. Figures 26a–f depict the DPBI for the event case and Figs. 27a–f depict the DPBI values for the non-event case. At 1200 UTC 26 November 1988 (Fig. 26a), the DPBI depicts large values (> 15) over AR, TX and LA until 2200 UTC 26. Storm data (NOAA, 1988) indicates there were numerous F0, F1 and F2 intensity tornadoes over that area at that time. The last funnel cloud over that area (MS) was at 2120 UTC. At 2100 UTC the DPBI over MS is > 15 . The index decreased significantly by 0000 UTC 27 November 1988 (Fig. 26b). After a period of time with low values (Figs. 26c–e) the values increase to over 15 at 0600 UTC 28 November 1988 over central NC. Over the entire 48 hour period of the non-event case, the maximum DPBI value is only 5. Storm data (NOAA, 1990) indicates there were no tornadoes over the southeast US for this time period. The DPBI predicts no severe weather over the Piedmont for the non-event (1800 UTC

25 to 0000 UTC 26 January 1990). Finally, the DPBI is being evaluated on a daily basis.

8. Summary and conclusions

In the six hours preceding the RDU tornado there was supergeostrophic upper-level flow (STJ exit region) over VA, NC and SC coastal region. At the same time, the PJ moved over the Appalachians so the PJ's right entrance region came in close proximity to the STJ's left exit region. The two associated transverse ageostrophic circulations juxtaposed (phased) creating a region of strong upper-level divergence and ascent over the Piedmont. For the non-event case, a PJ extended from TX northeast to the North Atlantic Ocean. There was no STJ over the eastern US thus there could be no phasing of jet streaks as in the event case.

In the mid-levels of the event case, the warm Mexican air ($> 330 \text{ K}$) at 850 hPa elevated the

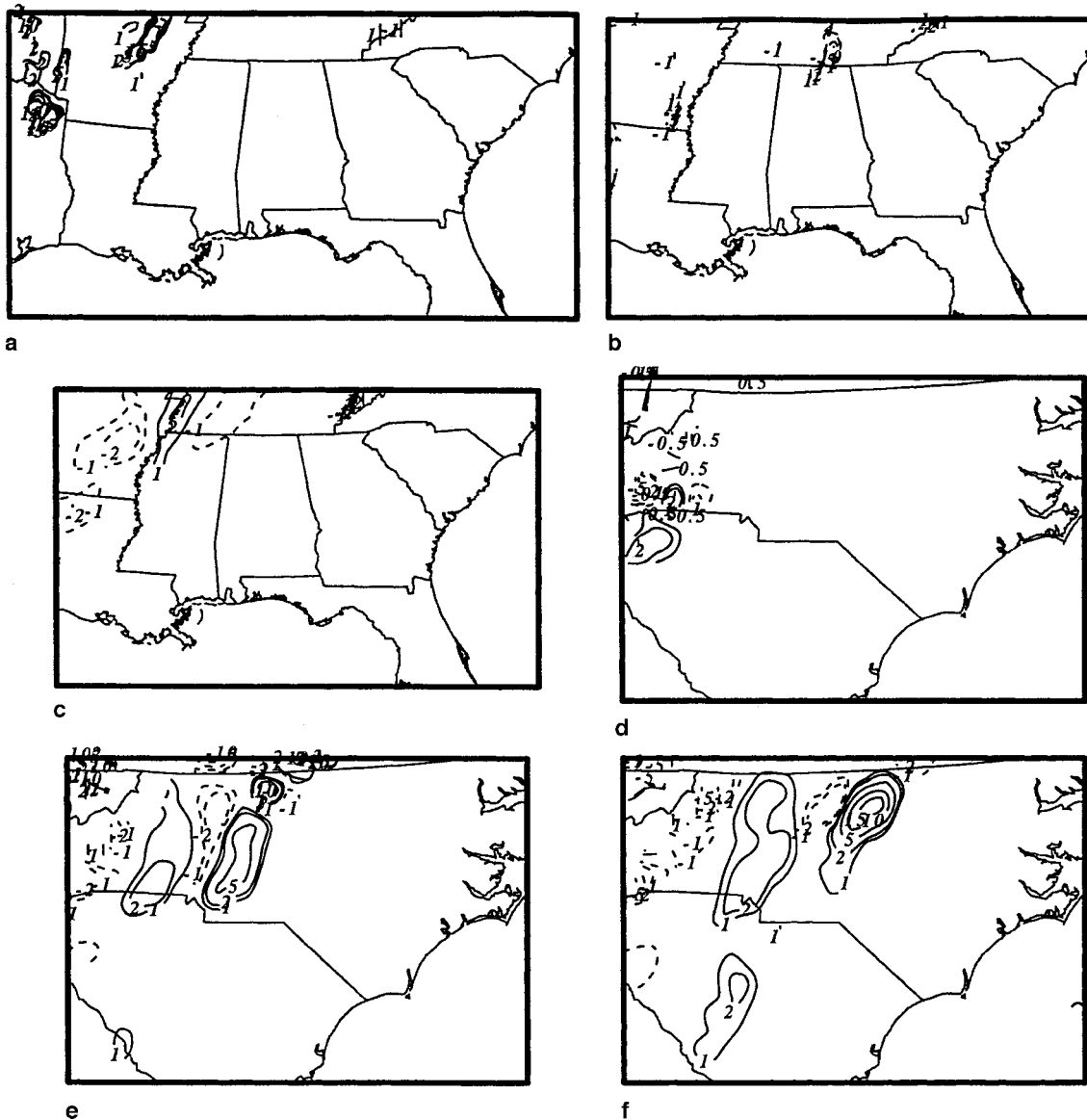


Fig. 26. MASS simulated, 24 km mesh, Divergence Profile Buoyancy Index. Solid lines indicate positive values and dashed lines indicate negative values (contoured $-15, -10, -5, -2, -1, 1, 2, 5, 10, 15, 20$) valid at **a** 1200 UTC 26, **b** 0000 UTC 27, **c** 1200 UTC 27, **d** 0000 UTC 28, **e** 0400 UTC 28, and **f** 0600 UTC 28 November 1988

heights to the southeast of the mid-level jet. The elevated heights in the right exit region increased the mid-level PGF and forced the continued development of the jet. The warm air also enabled the mid-level jet to be farther east than in a balanced QG system. As the jet accelerated it induced a thermally direct ageostrophic circulation with ascent over the warm MX air. This forcing mechanism was continually regenerated as the low-level baroclinic zone intensified and generated latent heating by convection. At the time of the tornado outbreak, the mid-level jet had intensified greatly and moved beneath the PJ

entrance region and the STJ exit region, which enhanced ascent. For the non-event case, a mid-level jet developed with the QG front/trough system over the Midwest US and moved north-eastward. In contrast to the event case, the 850 hPa, warm air from MX (>330 K) had not moved over the Piedmont. At the expected time of the non-event there was descent in the low-levels and very weak ascent in the mid-levels over the Piedmont.

The PV was examined for the last 6 hours for both the event and non-event. In the event case, the low-level PV maximum was closely related

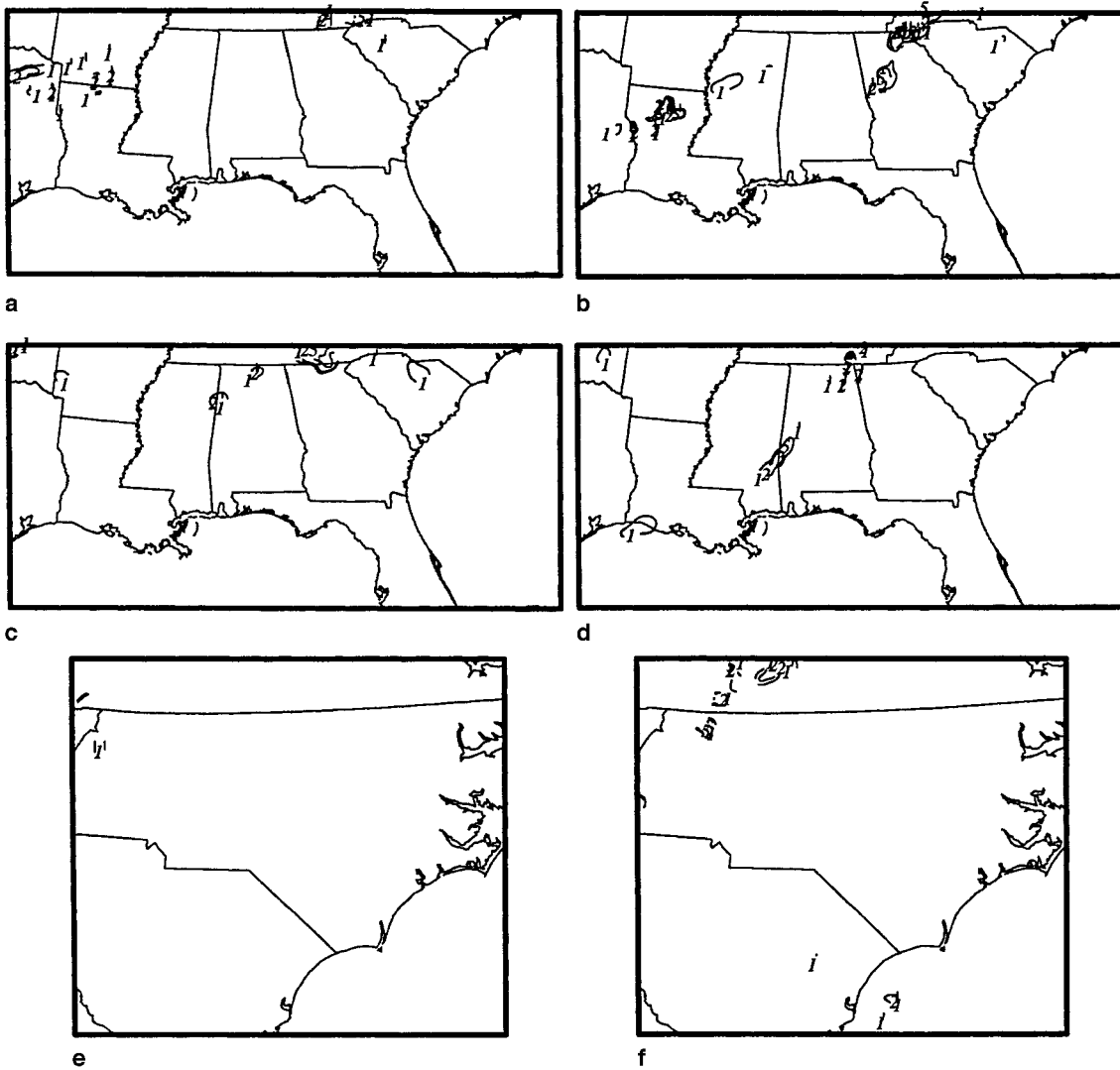


Fig. 27. MASS simulated, 24 km mesh, Divergence Profile Buoyancy Index. Solid lines indicate positive values and dashed lines indicate negative values (contoured $-15, -10, -5, -2, -1, 1, 2, 5, 10, 15, 20$) valid at **a** 0300 UTC 24, **b** 1500 UTC 24, **c** 0300 UTC 25, **d** 1500 UTC 25, **e** 1800 UTC 25, and **f** 0000 UTC 26 January 1990

to a mesocyclone (over the Piedmont) and with the areas of maximum trough deepening. The strongest PV was in the low-levels and the low-level PV maximum was decoupled from the upper-levels. Just as in the preceding 48 hours, the PV over the Piedmont was transported and/or generated in the low-levels. In the non-event, the low-level PV over NC and SC was very sporadic (generated by diabatic effects associated with convection).

We also noted a relationship between convection and low-level PV. Convection generates PV through diabatic heating; the low-level PV maxima increased, in large part, from latent heat energy associated with convection. One differ-

ence between these cases was that the event case had existing low-level PV maxima (traceable over 72 hours) so convection was a maintainer rather than primary generator of PV. In the non-event case, convection was the primary generator of low-level PV over the Piedmont.

The mesoscale model-generated data indicated the potential for severe weather for the event case, which is something the forecasters did not have at that time. Simulation-produced LI, SRH, low-level shear and wind imbalance as measured by the thermal wind were clearly different between the cases. All these parameters indicated the potential for severe weather in the event case and not in the non-event case.

We developed a new divergence profile buoyancy index based on: large scale synoptic features (upper-level divergence); mesoscale features (low-level tilting effects which incorporate shear and thermal gradients); and the buoyancy of the airmass. We found values over 15 corresponded to tornadic activity over both the MO, AK, TX, LA and MS (early in the period) and over central NC (late in the period).

The low-level potential vorticity in the event case could be traced from central NC at the time of the tornado outbreak back to its origins (some 84 hours earlier). The low-level PV facilitated the tracking of a mesoscale surface trough that developed over the western Gulf of Mexico, propagated northeastward along the Gulf Coast States, developed (merged) into a surface cold front and moved over the Piedmont at the time of the tornado outbreak. *The STJ was crucial to this 3-day process. First, it transported stratospheric PV rich air to the south then downward to the mid-levels over the Mexican plateau. Second, its associated ageostrophic circulation created upper-level divergence (mass removal from the air column) that helped to maintain deep convection and the surface trough. Third, it phased with the PJ creating intense upper-level divergence and ascent over the Piedmont.* At the same time, the warm low-level Mexican airmass propagated over the Gulf Coast States. The warm airmass was located to the southeast of the surface trough, and in conjunction with cold air advection to the northwest created an intense northwestward-directed PGF and a mid-level jet. The mid-level jet and its associated thermally direct ageostrophic circulation enhanced ascent over the low-level trough. These features created an environment favorable to deep convection and the release of latent heat that helped to maintain the low-level trough (confluence zone) and PV as it propagated along the Gulf Coast. Additionally, the latent heating, associated with convection, helped create an unbalanced jet with a thermally direct circulation in the jet exit region. The direct circulation associated with the mid-level jet facilitated convection ahead of the surface (over the warm air). The latent heating from convection and surface sensible heating helped maintain the surface front. Cold air advection from the northwest further enhanced the strength of the front. As air parcels moved over this front, they

encountered a very strong shear and thermal gradient, thus, they were tilted, generated vorticity and ascended rapidly.

Acknowledgements

The first author would like to thank the Air Force Institute of Technology for the opportunity to pursue my advanced degree. The authors wish to thank Drs Robert Rozumalski and Kenneth Waight III of MESO Inc. for access to and help with the MASS model.

References

- Bluestein HB (1993) Synoptic-Dynamic Meteorology in Midlatitudes, Vol II. Observations and Theory of Weather Systems. Oxford: Oxford University Press, 594 p
- Davies-Jones R, Burgess D, Foster M (1990) Test of helicity as a forecast parameter. Preprints 16th Conf. Severe Local Storms, Kananaskis, Alberta, Amer Meteor Soc 588–592
- Egentowich JM, Kaplan ML, Lin Y-L, Riordan AJ (1999a) Mesoscale simulations of dynamical factors discriminating between a tornado outbreak and non-event over the southeast US, part I: 84–48 hour precursors. Meteorol Atmos Phys (current issue)
- Egentowich JM, Kaplan ML, Lin Y-L, Riordan AJ (1999b) Mesoscale simulations of dynamical factors discriminating between a tornado outbreak and non-event over the southeast US, part II: 48–6 hour precursors. Meteorol Atmos Phys (current issue)
- Gidel LT, Shapiro MA (1979) The role of clear air turbulence in the production of potential vorticity in the vicinity of upper tropospheric jet stream-frontal systems. J Atmos Sci 36: 2125–2138
- Gonski RF, Woods BP, Korotky WD (1989) The Raleigh tornado – 28 November 1988: An operational perspective. Preprints, 12th Conf. on Weather Analysis and Forecasting, Monterey, CA Amer Meteor Soc, 173–178
- Gyakum JR, Kuo YH, Guo Z, Guo Y-R (1995) A case of rapid continental mesoscale cyclogenesis. Part II: Model and observational diagnosis. Mon Wea Rev 123: 998–1024
- Hamilton DW, Lin Y-L, Weglarz RP, Kaplan ML (1998) Jetlet formation from diabatic forcing with applications to the 1994 Palm Sunday tornado outbreak. Mon Wea Rev 126: 2061–2089
- Kaplan ML, Paine DA (1977) The observed divergence of the horizontal velocity field and pressure gradient force at the mesoscale. It's implications for the parameterization of three-dimensional momentum transport in synoptic-scale numerical models. Beitr Phy Atmos 50: 321–330
- Kaplan ML, Karyampudi VM (1992a) Meso-beta numerical simulation of terrain drag-induced along-stream circulations. Part I: Midtropospheric frontogenesis. Meteorol Atmos Phys 49: 133–156
- Kaplan ML, Karyampudi VM (1992b) Meso-beta numerical simulation of terrain drag-induced along-stream circulations. Part II: Concentration of potential vorticity within dryline bulges. Meteorol Atmos Phys 49: 157–185

- Kaplan ML, Zack JW, Wong VC, Tuccillo JJ (1982a) Initial results from a mesoscale atmospheric simulation system and comparisons with the AVE-SESAME I data set. *Mon Wea Rev* 110: 1564–1590
- Karyampudi VM, Kaplan ML, Koch SE, Zamora RJ (1995) The influence of the Rocky Mountains on the 13–14 April 1986 severe weather outbreak. Part I: Mesoscale lee cyclogenesis and its relationship to severe weather and dust storms. *Mon Wea Rev* 123: 1394–1422
- Kaplan ML, Lin Y-L, Hamilton DW, Rozumalski RA (1998) The numerical simulation of an unbalanced jetlet and its role in the Palm Sunday 1994 tornado outbreak in Alabama and Georgia. *Mon Wea Rev* 126: 2133–2165
- Kaplan ML, Rozumalski RA, Weglarz RP, Lin YL, Businger S, Gonski RF (1995) Numerical simulation studies of the mesoscale environment conducive to the Raleigh tornado. NOAA Tech. Memo ER-90, 1–101
- Lin Y-L, Wang T-A (1996) Flow regimes and transient dynamics of two-dimensional stratified flow over an isolated mountain ridge. *J Atmos Sci* 53: 139–158
- MESO (1995) MASS Version 5.8 Reference Manual, MESO, Troy, NY, 119 pp
- NOAA (1990) Storm data, 32, 01: 66 pp
- NOAA (1988) Storm data, 30, 11: 72 pp
- Zehnder JA, Keyser D (1991) The influence of interior gradients of potential vorticity on rapid cyclogenesis. *Tellus* 43A: 198–212

Corresponding author's address: Dr. Yuh-Lang Lin, Department of Marine, Earth and Atmospheric Sciences, North Carolina State University, Raleigh, NC (E-Mail: yl_lin@ncsu.edu)